JEM Journal of Experimental Medicine

ARTICLE

Histamine H_2 receptor negatively regulates oligodendrocyte differentiation in neonatal hypoxic-ischemic white matter injury

Lei Jiang*, Li Cheng*, Han Chen, Haibin Dai, Dadao An, Qianyi Ma, Yanrong Zheng, Xiangnan Zhang, Weiwei Hu, and Zhong Chen

Neonatal hypoxic-ischemic encephalopathy (HIE) with the pathological characteristic of white matter injury often leads to lifelong cognitive and neurobehavioral dysfunction, but relevant therapies to promote remyelination are still unavailable. We found that histamine H_2 receptor (H_2R) negatively regulated the oligodendrocyte differentiation rate without affecting the oligodendrocytes at the oligodendrocyte precursor cell stage or mature stage following oxygen-glucose deprivation in vitro. Notably, selective deletion of the H_2R gene (*Hrh2*) in differentiating oligodendrocytes (*Hrh2*$^{fl/fl}$*;CNPase-Cre*) improved their differentiation, remyelination, and functional recovery following neonatal hypoxia-ischemia in mice. The regulation of oligodendrocyte differentiation by H_2R is mediated by binding with Axin2, which leads to up-regulation of the Wnt/β-catenin signaling pathway. Furthermore, H_2R antagonists also promoted oligodendrocyte differentiation and remyelination and the recovery of cognition and motor functions following neonatal hypoxia-ischemia. Thus, histamine H_2R in oligodendrocytes could serve as a novel and effective therapeutic target for the retard of oligodendrocyte differentiation and remyelination following neonatal hypoxia-ischemia. The H_2R antagonists may have potential therapeutic value for neonatal HIE.

Introduction

Neonatal hypoxic-ischemic (HI) encephalopathy (HIE) in newborns has a prevalence of 0.1–0.8% and may lead to cerebral palsy and lifelong neurobehavioral dysfunction (Kurinczuk et al., 2010). Relevant therapies to promote functional recovery from HIE are still unavailable (Douglas-Escobar and Weiss, 2015). The major pathological change in neonatal HIE is white matter injury (WMI), with the characteristics of demyelination and insufficient numbers of mature oligodendrocytes (OLs), especially for premature infants (Khwaja and Volpe, 2008; Yildiz et al., 2017). The demyelinated lesions can be rescued by remyelination, which results from the recruitment of OL precursor cells (OPCs) and subsequent differentiation. Such remyelination has been found in inflammatory WMI, such as in the progress of multiple sclerosis or experimental allergic encephalomyelitis (Blakemore and Franklin, 2008; Franklin and Ffrench-Constant, 2008). However, the remyelination fails in neonatal HIE, resulting in ongoing neurological dysfunction, axonal loss, and disease progression. The number of OPCs was increased in demyelinated regions induced by HI in neonatal mice, but their differentiation into mature OLs was impeded (Billiards et al., 2008; Buser et al., 2012; Fancy et al., 2014; Segovia et al., 2008). Thus, promotion of OL differentiation might rescue hypomyelination defects and yield improved clinical outcomes (Fancy et al., 2011; Wang et al., 2018); however, very few drug targets that are manipulatable for OL differentiation have been identified.

Histamine regulates sleep, wakefulness, learning, memory, and food intake in its roles as a neurotransmitter or neuromodulator (Panula and Nuutinen, 2013; Passani et al., 2014). Histamine H_2 receptor (H_2R) is widely distributed in the mammalian brain with high expression (Hill et al., 1997), including in the basal ganglia, hippocampus, amygdala, and cerebral cortex (Traiffort et al., 1992). In the present study, we for the first time identified H_2R expression in all stages of OLs in vivo and in vitro, and the expression was altered following postnatal HI. To examine the functional role of H_2R in neonatal HI WMI, we selectively deleted H_2R in differentiating OLs (*Hrh2*$^{fl/fl}$*;CNPase-Cre*) by crossing *Hrh2*$^{fl/fl}$ mice with *CNPase-Cre* mice. We demonstrated that H_2R negatively regulates OL differentiation following neonatal HI using *Hrh2*$^{fl/fl}$*;CNPase-Cre*

Department of Pharmacology and Department of Pharmacy of the Second Affiliated Hospital, National Health Commission and Chinese Academy of Medical Sciences Key Laboratory of Medical Neurobiology, Department of Anatomy, School of Basic Medical Science, Zhejiang University School of Medicine, Hangzhou, China.

*L. Jiang and L. Cheng contributed equally to this paper; Correspondence to Weiwei Hu: huww@zju.edu.cn.

mice, or by adeno-associated virus (AAV)–mediated overexpression or knockdown of H_2R in vivo and in vitro. These results suggest that H_2R in OLs is likely essential for the retard of OL differentiation and remyelination in the pathological progress of neonatal HIE and serves as a novel and effective therapeutic target. H_2R antagonists that have been used for gastroesophageal reflux in preterm and full-term infants (Slaughter et al., 2016) may also have translational value for the treatment of neonatal HIE.

Results

H_2R expression in the OL lineages and in the white matter following neonatal HI

We first aimed to determine the expression pattern of H_2R in OLs in vitro and in vivo. H_2R protein expression was detectable in OL lineages, including $NG2^+$ OPCs, $O4^+$ differentiating OLs, and $CC\text{-}1^+$ or myelin basic protein $(MBP)^+$ mature OLs in vitro by immunocytochemistry (Fig. S1 a). The studies of RNAscope in situ hybridization and immunostaining for H_2R in the white matter corpus callosum of mouse brain validated that most $NG2^+$ OPCs, $O4^+$ or 2′,3′-cyclic-nucleotide 3′-phosphodiesterase $(CNP)^+$ differentiating OLs, or $CC\text{-}1^+$ mature OLs express H_2R (Fig. S1, b–d and f). Moreover, the mRNA or protein expression of H_2R was higher in differentiating OLs or mature OLs than that in OPCs (Fig. S1, b, c, e, and f). To determine whether H_2R expression in white matter is altered after neonatal HI, we evaluated H_2R protein expression by Western blot at 1 d, 7 d, 14 d, and 28 d after surgery (Fig. S1 g). The results showed that H_2R expression was significantly decreased at 1 d, but gradually increased to reach a significant elevation at 28 d compared with those in the sham group, along with a physiological decrease of H_2R expression during this development stage from postnatal weeks 1 to 5. The alteration of H_2R mRNA expression in OLs detected from an RNAscope in situ hybridization study was identical to that in the white matter tested by Western blot (Fig. S1, g, i, and k). The alteration of H_2R expression implies that H_2R in OLs may participate in the WMI induced by neonatal HI. However, the H_2R mRNA expression in either astrocytes or microglia was only 32.01 ± 5.786% (n = 5) or 37.58 ± 4.59% (n = 5) of that in $Olig2^+$ OLs, respectively, and remained unchanged following neonatal HI (Fig. S1, j and l–n). Moreover, we cannot observe the H_2R mRNA expression in platelet-derived growth factor (PDGF) receptor (PDGFR)β^+ pericytes at the neonatal age (Fig. S1 o). Meanwhile, the histamine content in the corpus callosum of the HI group was comparable to that in controls, although a gradual increase at this development stage was observed in both groups (Fig. S1 h).

H_2R negatively regulates OL differentiation after oxygen-glucose deprivation (OGD) in vitro

To investigate the role of H_2R in OL lineage progression following OGD–induced damage, different stages of OLs were infected with AAV-mediated overexpression (AAV-Hrh2) or knockdown (AAV-sh-Hrh2) of H_2R in vitro (Fig. 1 and Fig. S2 a). Both viruses exhibited effective overexpression or knockdown in primary cultured OL cells and the oli-neu cell line (Fig. S2, b and c). After infection, cells were exposed to 2 h OGD and displayed a reduced viability at 24 h after OGD (Fig. 1, a1, a2, b1, b2, c1, c2, d1, d2, e1, and e2). We found that neither overexpression nor knockdown of H_2R had an effect on the OPC pool quantified by $NG2^+$ OPC numbers and NG2 protein expression (Fig. 1, a1–a3), or the differentiation of OPCs into $O4^+$ multipolar differentiating OLs (Fig. 1, b1 and b2). Interestingly, overexpression of H_2R during the premyelinating stage significantly decreased the number of $O4^+$ multipolar differentiating OLs, while knockdown of H_2R robustly increased the number of these OLs (Fig. 1, c1 and c2). Similarly, overexpression or knockdown of H_2R during the immature stage also altered the $CC\text{-}1^+$ or MBP^+ mature OL numbers from the immunocytochemistry or Western blot analysis (Fig. 1, d1–d5). Meanwhile, overexpression and knockdown of H_2R during the premyelinating or immature stage had no effect on the total number of OLs ($Olig2^+$) after OGD (Fig. S2, d1–d3). It suggests that H_2R may negatively regulate OL differentiation after OGD. In addition, neither overexpression nor knockdown of H_2R during the mature stage affected the MBP^+ multipolar mature OLs after OGD insult (Fig. 1, e1 and e2).

Furthermore, the morphological complexity of differentiating OL processes was quantified using Sholl analysis (Fig. 1, c1 and c3), since OLs convert from a simple bipolar morphology to a complex branched morphology during differentiation (Rajasekharan et al., 2009). Knockdown of H_2R significantly increased the number of intersections made by the outer circle with the longer processes (three units), indicating promotion of differentiation in morphology, while overexpression of H_2R induced the opposite effect. To study the direct effect of H_2R on the OL differentiation process after OGD, we evaluated the time course change of the numbers of $O4^+$ (MBP^-) multipolar differentiating OLs and MBP^+ multipolar mature OLs after knockdown of H_2R (AAV-sh-Hrh2) during the premyelinating stage (Fig. 1, f1 and f3). The results showed that knockdown of H_2R increased the number of $O4^+$ OLs following OGD/reperfusion (3 d differentiated from OPCs), while the number of MBP^+ OLs was unchanged. With the incubation time extended, knockdown of H_2R gradually increased the number of MBP^+ OLs, but reduced the number of $O4^+$ OLs. Furthermore, the ratio of MBP^+ OL numbers to $O4^+$ OL numbers was calculated to directly analyze the differentiation rate (Fig. 1 f2). We found that the differentiation rate of OGD groups was lower than that of controls; however, knockdown of H_2R significantly increased the differentiation rate. It suggests that deficiency of H_2R promotes OL differentiation through the acceleration of differentiation rate after OGD.

To exclude a possible effect on the cell survival or apoptosis in premyelinating OLs (preOLs) induced by modulating H_2R expression, cell viability in the 3-(4,5-dimethylthiazol-2-yl)-2,5-diphenyltetrazolium bromide (MTT) assay, cleaved-caspase 3 expression, and terminal deoxynucleotidyl transferase dUTP nick end labeling (TUNEL) staining were performed (Fig. S2, e1, e2, f, and g). We found that neither overexpression nor knockdown of H_2R during the premyelinating stage affected viability and apoptosis after OGD insult. In addition, neither overexpression nor knockdown of H_2R during the premyelinating or immature stage affected the number of $O4^+$ multipolar

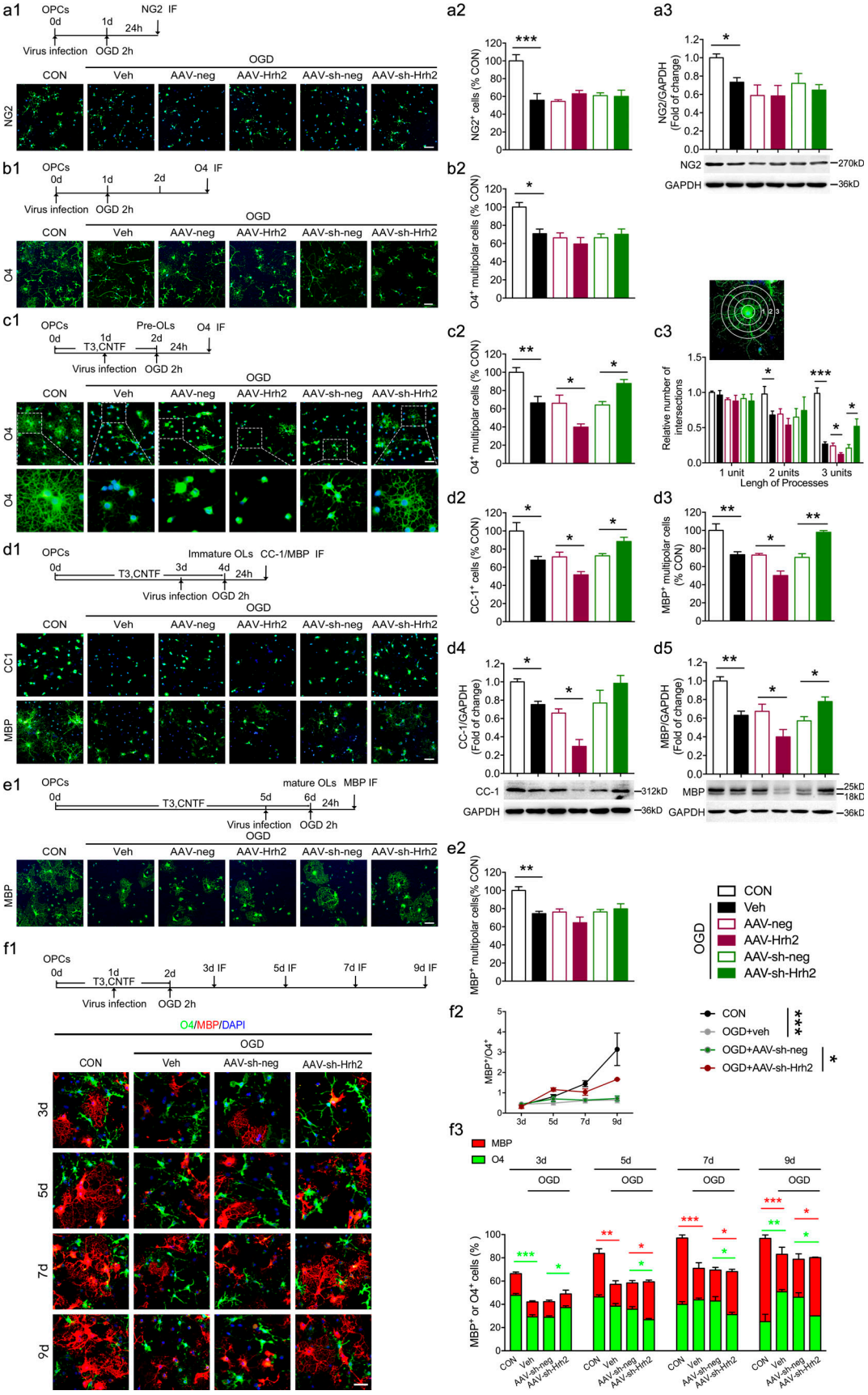

Figure 1. **H_2R negatively regulates OL differentiation following OGD in vitro. (a1–a3)** The primary cultured OPCs or oli-neu cells were infected with AAV-Hrh2 or AAV-sh-Hrh2 and subjected to OGD/reperfusion. Immunocytochemical visualization (a1) and the quantification of numbers of NG2+ OPCs (a2) at 24 h

after reperfusion. **(a3)** Western blot analysis of NG2$^+$ expression in oli-neu cells at 24 h after reperfusion. **(b1 and b2)** The primary cultured OPCs were infected with AAV-Hrh2 or AAV-sh-Hrh2 and subjected to OGD/reperfusion. Immunocytochemical visualization (b1) and the quantification of numbers of O4$^+$ multipolar cells (b2) at 2 d after reperfusion. **(c1–c3)** The primary cultured OPCs were differentiated into preOLs with incubation in T3 (40 ng/ml) and CNTF (10 ng/ml) for 2 d. The preOLs infected with AAV-Hrh2 or AAV-sh-Hrh2 were subjected to OGD/reperfusion. Immunocytochemical visualization (c1) and the quantification of numbers of O4$^+$ multipolar OLs (c2) at 24 h after reperfusion. The cells in the box portion in c1 were enlarged in the bottom panel. **(c3)** The process extensions for O4$^+$ multipolar OLs were analyzed using Sholl analysis. Branching was quantified by measuring the number of intersections that processes made with concentric circles, which are numbered 1–3 to reflect increasing distance from the cell body. **(d1–d5)** The primary cultured OPCs or oli-neu cells were differentiated into immature OLs with incubation in T3 (40 ng/ml) and CNTF (10 ng/ml) for 4 d. The immature OLs infected with AAV-Hrh2 or AAV-sh-Hrh2 were subjected to OGD/reperfusion. Immunocytochemical visualization (d1) and the quantification of numbers of CC-1$^+$ mature OLs (d2) or MBP$^+$ multipolar mature OLs (d3) at 24 h after reperfusion. **(d4 and d5)** Western blot analysis of CC-1$^+$ and MBP$^+$ expression in oli-neu cells at 24 h after reperfusion. **(e1 and e2)** The primary cultured OPCs were differentiated into mature OLs with incubation in T3 (40 ng/ml) and CNTF (10 ng/ml) for 6 d. The mature OLs infected with AAV-Hrh2 or AAV-sh-Hrh2 were subjected to OGD/reperfusion. Immunocytochemical visualization (e1) and the quantification of numbers of MBP$^+$ multipolar mature OLs (e2) at 24 h after reperfusion. **(f1–f3)** The primary cultured OPCs were differentiated into preOLs with incubation in T3 (40 ng/ml) and CNTF (10 ng/ml) for 2 d. The preOLs infected with AAV-sh-Hrh2 were subjected to OGD/reperfusion. Immunocytochemical visualization (f1) and the quantification of percentage of O4$^+$ (MBP$^-$) multipolar OLs and MBP$^+$ multipolar OLs (f3) at 1 d, 3 d, 5 d, and 7 d after reperfusion (3 d, 5 d, 7 d, and 9 d differentiated from OPCs). **(f2)** The ratio of the MBP$^+$ multipolar OL numbers to O4$^+$ (MBP$^-$) multipolar OL numbers. Green: NG2 labels OPCs in a1; O4 labels preOLs in b1, c1, or f1; CC-1 and MBP label mature OLs in d1 or e1. Red, MBP labels mature OLs in f1; blue, DAPI. Scale bar, 50 µm. n = 4–6 from at least three independent experiments. *, P < 0.05; **, P < 0.01; ***, P < 0.001. The red asterisks represent the P value of the change in the numbers of MBP$^+$ multipolar mature OLs, and the green asterisks represent the P value of the change in the numbers of O4$^+$ (MBP$^-$) multipolar differentiating OLs in f3. CON, control; IF, immunofluorescence staining; Veh, vehicle.

differentiating OLs or MBP$^+$ multipolar mature OLs that had not been exposed to OGD (Fig. S2, h1–h3 and i). Taken together, these results suggest that H_2R decelerates the differentiation rate of differentiating OL under the setting of OGD without affecting the OLs at the OPC stage or mature stage.

H_2R negatively regulates OL differentiation and remyelination in lysolecithin (LPC)-induced WMI in mice

Remyelination is a biological process of recapitulation of myelination, which requires differentiation from OPCs into mature OLs (Franklin and Ffrench-Constant, 2008). To test whether H_2R also regulates the OL differentiation in vivo that eventually contributes to remyelination, we introduced the LPC-induced WMI model in adult mice, which is a useful model to examine demyelination and remyelination processes in the central nervous system. The rapid loss of myelin in the majority of OLs occurs with 2–3 d postlesion (dpl) induced by LPC injection, while OPC recruitment (5 dpl), differentiation (10 dpl), and myelination (14 dpl) are subsequently observed in the impaired white matter (Blakemore and Franklin, 2008; Fancy et al., 2011). We characterized the demyelinated area by MBP staining the corpus callosum at 10 dpl to evaluate whether knockdown or overexpression of H_2R induction affected myelination (Fig. S3, a1 and a2). The quantitative analysis revealed that overexpression of H_2R (AAV-Hrh2) significantly increased the LPC-induced demyelinated area, while knockdown of H_2R (AAV-sh-Hrh2) decreased the demyelinated area. The number of NG2$^+$ OPCs in demyelinated lesions was unchanged following AAV-Hrh2 or AAV-sh-Hrh2 injection (Fig. S3, a1 and a3), suggesting no effect of H_2R on OPCs. This result implies that H_2R might impede remyelination through blocking OL differentiation.

To verify the role of H_2R in the differentiation of OLs, we deleted the H_2R gene in differentiating OLs by crossing the *CNPase-Cre* line with the mice whose *Hrh2* allele was flanked by loxp sites (*Hrh2$^{fl/fl}$;CNPase-Cre*). *Hrh2$^{fl/fl}$;CNPase-Cre* mice displayed deficient *Hrh2* mRNA expression in O4$^+$ or CNP$^+$ differentiating OLs, but not in NG2$^+$ OPCs, by RNAscope in situ hybridization with immunostaining (Fig. 2 a). *Hrh2$^{fl/fl}$;CNPase-Cre* mice exhibited a comparable size of demyelinated area in the corpus callosum at 5 dpl in MBP staining, but a reduced demyelinated area compared with *Hrh2$^{fl/fl}$* control mice in Luxol fast blue (LFB) and MBP staining at 10 dpl (Fig. 2, b and f–h). It suggests that selective deletion of H_2R in differentiating OLs promotes remyelination in LPC-induced myelin injury. Moreover, there is no difference in proliferation (Ki67$^+$ and PDGFRα$^+$ cells) and recruitment of OPCs into lesions (either NG2$^+$ or PDGFRα$^+$ cells) between *Hrh2$^{fl/fl}$;CNPase-Cre* mice and *Hrh2$^{fl/fl}$* control mice (Fig. 2, b, d, i, k, and l). The improved remyelination in *Hrh2$^{fl/fl}$;CNPase-Cre* mice could result from an elevated differentiation of OLs (Fig. 2, c and j) rather than from affecting OL apoptosis (TUNEL$^+$ and Olig2$^+$ cells; Fig. 2, e and m).

To further validate the role of H_2R in OL differentiation, a Cre-dependent AAV containing floxed Hrh2-GFP (AAV-FLEX-Hrh2) was injected into the corpus callosum of *Hrh2$^{fl/fl}$;CNPase-Cre* mice to selectively reexpress H_2R in differentiating OLs (Fig. 2, n and o). The immunostaining revealed that 95.30 ± 4.55% of GFP-labeled cells were CNP$^+$ OLs, and 80.88 ± 9.35% of CNP$^+$ OLs were infected with AAV-FLEX-Hrh2 (n = 4). In situ hybridization of H_2R mRNA validated that 79.21 ± 5.27% of CNP$^+$ OLs effectively expressed H_2R (n = 4; Fig. 2 o). Consistent with the findings shown in Fig. 2, b, h, and j, *Hrh2$^{fl/fl}$;CNPase-Cre* mice injected with control virus (AAV-FLEX-neg) showed improved OL differentiation and remyelination in the lesion area (Fig. 2, p, q, and s–u). However, selective reexpression of H_2R (AAV-FLEX-Hrh2) in differentiating OLs completely reversed all of the alterations in *Hrh2$^{fl/fl}$;CNPase-Cre* mice (Fig. 2, p, q, and s–u). Moreover, selective reexpression of H_2R had no effect on the OPC pool (Fig. 2, p and r). Taken together, these data provide solid evidence that blocking H_2R in OLs can accelerate their differentiation to promote remyelination without affecting OL proliferation or apoptosis.

To investigate whether H_2R in microglia or astrocytes was also involved in remyelination, we selectively overexpressed H_2R in microglia by injection of a Cre-dependent lentivirus, Lenti-FLEX-Hrh2, into the corpus callosum of *CX3CR1-CreER* mice, or overexpressed or knocked down H_2R in astrocytes by

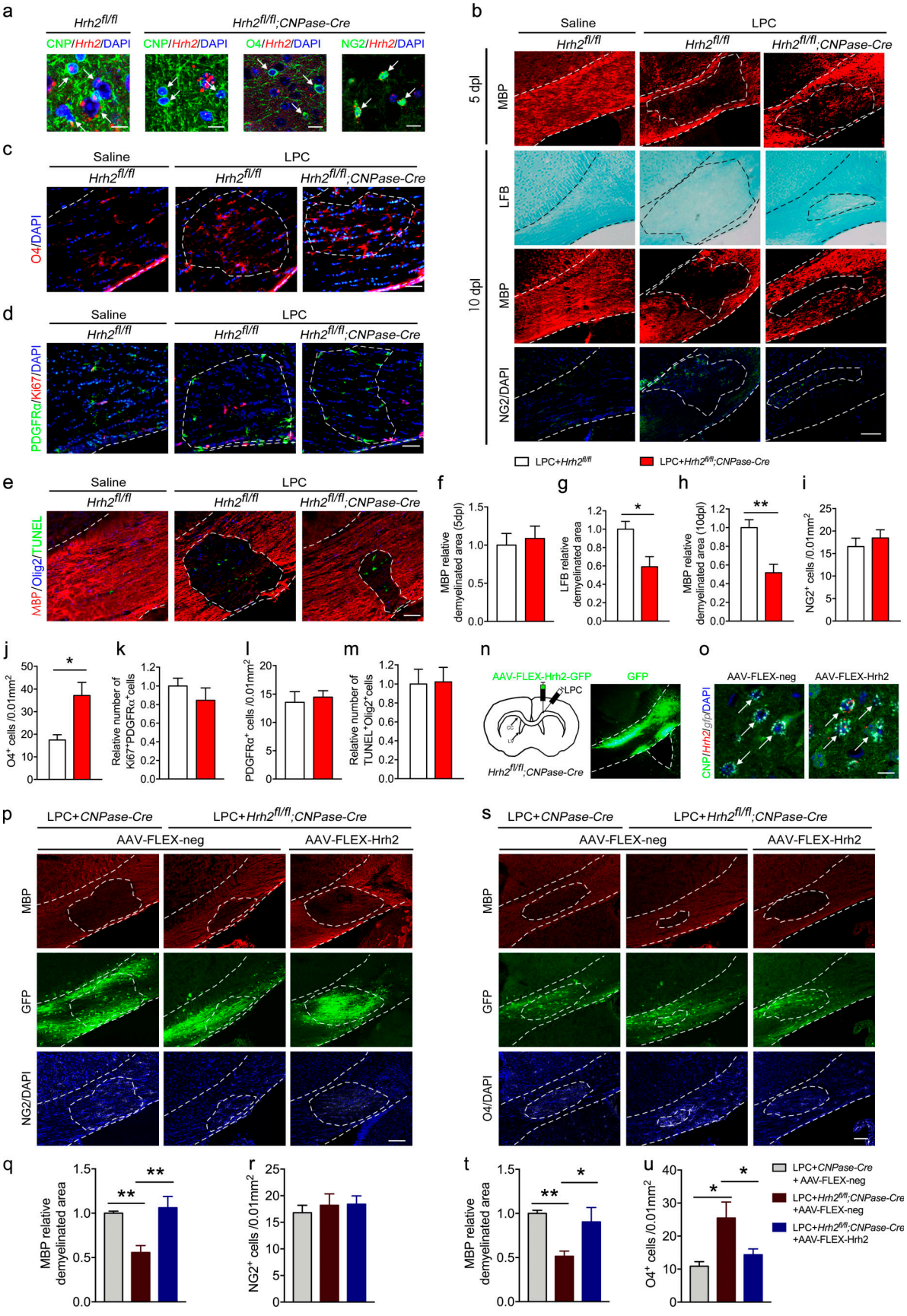

Figure 2. **Selective deletion of H_2R in differentiating OLs promotes OL differentiation and remyelination in LPC-induced WMI. (a)** To specifically delete *Hrh2* in differentiating OLs, *Hrh2*$^{fl/fl}$ homozygous mice were mated with *CNPase-Cre* mice to generate *Hrh2*$^{fl/fl}$*;CNPase-Cre* mice. In situ hybridization of *Hrh2*

mRNA by RNAscope together with immunostaining of CNP, O4, or NG2 and visualization of nuclei by DAPI in the corpus callosum to confirm the deletion of H_2R in differentiating OLs, but not in OPCs. Scale bar, 20 µm. **(b–m)** *Hrh2$^{fl/fl}$;CNPase-Cre* mice and *Hrh2$^{fl/fl}$* control mice were subjected to LPC injections in the corpus callosum. Representative images (b) and quantification of demyelinated area in MBP staining (f and h) and LFB staining (g), as well as numbers of NG2$^+$ OPCs in the LPC-induced demyelinated area (i) at 5 d or 10 dpl. Red, MBP; green, NG2; blue, DAPI. *n* = 4–6 mice for each group from at least three independent experiments. Scale bar, 100 µm. Immunohistochemical visualization (c–e) and quantification of O4$^+$ preOLs (j), OPC proliferation (Ki67 and PDGFRα colabeled cells, k), OPC numbers (PDGFRα labeled cells, l), and OL apoptosis (TUNEL and Olig2 colabeled cells, m) at 10 dpl. *n* = 4 or 5 mice for each group from at least two independent experiments. Scale bar, 50 µm. **(n–s)** Cre-dependent AAV containing floxed Hrh2-GFP (AAV-FLEX-Hrh2-GFP) was injected into the corpus callosum of *Hrh2$^{fl/fl}$;CNPase-Cre* mice to selectively reexpress H_2R in differentiating OLs. **(n)** Schematic diagram of microinjection of AAV-FLEX-Hrh2 and LPC in the corpus callosum of *Hrh2$^{fl/fl}$;CNPase-Cre* mice, and representative images of Hrh2-GFP expression in the corpus callosum of *Hrh2$^{fl/fl}$;CNPase-Cre* mice. **(o)** In situ hybridization of *Hrh2* and *gfp* mRNA by RNAscope, immunostaining of CNP, and visualization of nuclei by DAPI in the corpus callosum to confirm the reexpression H_2R in differentiating OLs. Arrows indicate the AAV-FLEX-Hrh2–infected OLs. Scale bar, 20 µm. **(p–r)** Immunohistochemical visualization (p) and quantification of demyelinated area in MBP staining (q) and NG2$^+$ OPC numbers in LPC-induced demyelinated area (r) of *Hrh2$^{fl/fl}$;CNPase-Cre* mice injected with AAV-FLEX-Hrh2-GFP or AAV-FLEX-GFP as control. Red, MBP; green, GFP; gray, NG2; blue, DAPI. **(s–u)** Immunohistochemical visualization (s) and quantification of demyelinated area in MBP staining (t) and O4$^+$ differentiating OL numbers in LPC-induced demyelinated area (u) of *Hrh2$^{fl/fl}$;CNPase-Cre* mice injected with AAV-FLEX-Hrh2-GFP or AAV-FLEX-GFP as control. Red, MBP; green, GFP; gray, O4; blue, DAPI. Scale bar, 100 µm. *n* = 5 mice for each group from three independent experiments. *, P < 0.05; **, P < 0.01. The areas outlined by a dashed line indicate the quantified areas in the corpus callosum.

injection of AAV-FLEX-Hrh2 or AAV-FLEX-sh-Hrh2 in *GFAP-Cre* mice (Fig. S3, c1 c2, d1, and d2). In *CX3CR1-CreER* mice, 94.73 ± 4.82% of Lenti-FLEX-Hrh2–infected cells are Iba-1$^+$ microglia, and 71.90 ± 7.62% of microglia were infected with Lenti-FLEX-Hrh2 (*n* = 4). In *GFAP-Cre* mice, 92.85 ± 1.43% of AAV-FLEX-Hrh2–infected cells were GFAP$^+$ astrocytes, and 84.21 ± 5.26% of astrocytes were infected with AAV-FLEX-Hrh2; meanwhile, 94.73 ± 2.84% of AAV-FLEX-sh-Hrh2–infected cells were GFAP$^+$ astrocytes, and 85.71 ± 2.86% of astrocytes were infected with AAV-FLEX-sh-Hrh2 (*n* = 4). We found that overexpression or knockdown of H_2R either in microglia or astrocytes had no effect on the demyelinated area at 10 dpl in the LPC model. It suggests that H_2R in microglia or astrocytes may not be involved in the remyelination following LPC-induced myelin injury.

Deletion of H_2R in differentiating OLs promotes their differentiation and remyelination in neonatal HI mice

To further elucidate whether H_2R in differentiating OLs is involved in remyelination in neonatal HI WMI, *Hrh2$^{fl/fl}$;CNPase-Cre* and *Hrh2$^{fl/fl}$* neonates were subjected to HI. MBP expression and NG2$^+$ OPCs in the corpus callosum of *Hrh2$^{fl/fl}$;CNPase-Cre* mice were comparable to those in *Hrh2$^{fl/fl}$* mice at 7 d after HI (Fig. 3, a1–a3), suggesting that deletion of H_2R in differentiating OLs did not affect demyelination and OPC number. An increased number of O4$^+$ differentiating OLs was observed in the corpus callosum of *Hrh2$^{fl/fl}$;CNPase-Cre* mice compared with *Hrh2$^{fl/fl}$* mice at 14 d after HI (Fig. 3, a1 and a4). Furthermore, MBP expression was enhanced in the corpus callosum of *Hrh2$^{fl/fl}$;CNPase-Cre* mice at 28 d after HI (Fig. 3, a1 and a5). These results suggest that deletion of H_2R in differentiating OLs is capable of facilitating their differentiation and maturation following HI.

To test whether increased mature OLs contributed to axonal remyelination in *Hrh2$^{fl/fl}$;CNPase-Cre* mice, we performed immunofluorescent double staining for MBP and neurofilament marker NF200. The results showed that deleting H_2R in differentiating OLs significantly enhanced the ratio of MBP to NF200 at 28 d after HI (Fig. 3, b1 and b2), suggesting high axonal remyelination. Scanning electron microscopy also showed that the myelinated axons were elevated in *Hrh2$^{fl/fl}$;CNPase-Cre* mice in contrast to *Hrh2$^{fl/fl}$* mice in the corpus callosum (Fig. 3, c1 and c2). Moreover, the myelin sheaths in *Hrh2$^{fl/fl}$;CNPase-Cre* mice were thicker (i.e., decreased g-ratio, the ratio between the inner and the outer diameter of the myelin sheath) compared with *CNPase-Cre* mice after neonatal HI, but they were still thinner than that in *Hrh2$^{fl/fl}$;CNPase-Cre* mice without HI (i.e., increased g-ratio; Fig. 3 c3). Since the thin myelin sheaths are recognized as remyelination (Duncan et al., 2017; Franklin and Goldman, 2015), the g-ratio analysis further supports that deletion of H_2R in differentiating OLs promotes the remyelination after neonatal HI.

Furthermore, mice were subjected to motor coordination and cognitive tests from 28 d to 35 d following HI. *Hrh2$^{fl/fl}$;CNPase-Cre* mice showed significant improvement of motor coordination with prolonged latency to fall from a rotating cylinder in rotarod tests (Fig. 3 e). Since the corpus callosum is related to the cognitive behavior pertaining to both the nonspatial and spatial memory, mice were subjected to cognitive tests including object recognition tests and Morris water maze tests (Miu et al., 2006; Zhou et al., 2017). The *Hrh2$^{fl/fl}$* mice showed a robust decrease in discriminative ability in the object recognition tests after HI, while *Hrh2$^{fl/fl}$;CNPase-Cre* mice exhibited significant improvements in the discrimination index (Fig. 3 d). In the Morris water maze tests, the *Hrh2$^{fl/fl}$* mice exposed to HI displayed longer escape latencies during the acquisition trials but spent less time searching in the quadrant that previously had the platform in the probe trial, revealing spatial memory impairments. However, *Hrh2$^{fl/fl}$;CNPase-Cre* mice had intact spatial memory in the acquisition trials and probe trial (Fig. 3, f1–f3). The average swim speed showed no differences among all groups (Fig. 3 f4). In addition, there were no differences of motor coordination and cognitive ability between the *Hrh2$^{fl/fl}$* and *Hrh2$^{fl/fl}$;CNPase-Cre* mice without HI insult (Fig. 3, d, e, and f1–f4). These observations reveal that the deletion of H_2R in differentiating OLs promotes their differentiation to benefit remyelination and the recovery from motor coordination and cognitive impairment following neonatal HI.

H_2R negatively regulates OL differentiation through the Wnt/β-catenin signaling pathway

It is generally understood that the downstream cascade of H_2R constitutive activity coupled to Gs proteins stimulates adenylyl

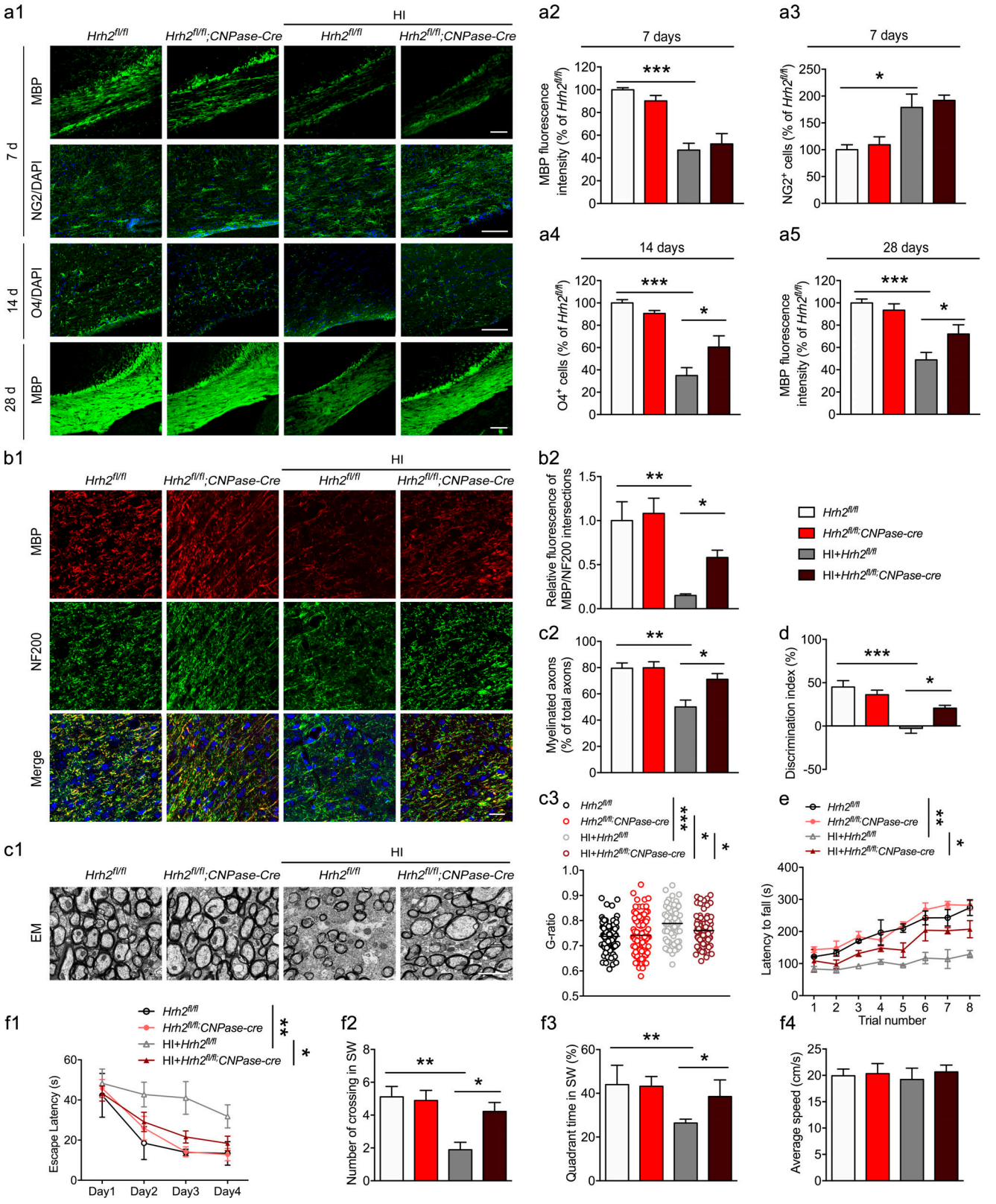

Figure 3. **Selective deletion of H_2R in differentiating OLs promotes OL differentiation, remyelination, and functional recovery in neonatal HI mice.** *Hrh2*$^{fl/fl}$*;CNPase-Cre* and *Hrh2*$^{fl/fl}$ neonates were subjected to unilateral common carotid artery ligation plus inhalational hypoxia. **(a1–a5)** Immunohistochemical visualization and quantification of MBP expression and NG2$^+$ OPC numbers at 7 d, O4$^+$ differentiating OL numbers at 14 d, as well as MBP expression at 28 d after HI. *n* = 5–7 mice for each group from at least three independent experiments. Scale bars, 100 µm. **(b1 and b2)** Immunohistochemical visualization and quantification of colocalization of MBP and NF200 in the corpus callosum of *Hrh2*$^{fl/fl}$*;CNPase-Cre* and *Hrh2*$^{fl/fl}$ mice at 28 d after HI. *n* = 5 mice for each group from three independent experiments. Scale bar, 50 µm. **(c1–c3)** Representative images, the percentage of myelinated axon fibers, and the g-ratio of myelinated

axons in the corpus callosum from electron microscopy at 28 d after HI. *n* = 3 mice for each group from two independent experiments in c1 and c2; *n* = 74–109 axons for each group from three mice. Scale bar, 2 µm. **(e)** Motor coordination evaluated by the latency to fall from a rotating cylinder in rotarod tests in *Hrh2*$^{fl/fl}$*;CNPase-Cre* and *Hrh2*$^{fl/fl}$ mice at day 28 after HI. Cognitive behavior was evaluated by discrimination index in object recognition test (d) and by Morris water maze test (f1–f4) for *Hrh2*$^{fl/fl}$*;CNPase-Cre* and *Hrh2*$^{fl/fl}$ mice from 28 d to 35 d after HI. **(f1)** Latency to reach the platform during the acquisition trial. **(f2 and f3)** Searching time (f2) and crossing number (f3) in the SW quadrant (target quadrant) in the probe trial. **(f4)** Average speed in the probe trial. *n* = 8–10 mice for each group from at least three independent behavior experiments. *, P < 0.05; **, P < 0.01; ***, P < 0.001. EM, electron microscopy.

cyclase (AC) and increases intracellular cAMP, which activates protein kinase A and the transcription factor cAMP response element–binding protein (CREB; Haas et al., 2008). We thus determined whether the AC/cAMP/CREB pathway is involved in the action of H_2R on OL differentiation (Fig. S4). OGD insult reduced CREB phosphorylation in oli-neu cells, while H_2R overexpression increased CREB phosphorylation, which was reversed by AC inhibitor SQ22536 (Fig. S4 a). However, SQ22536 had no effect on the decrease in O4$^+$ multipolar differentiating OL number induced by AAV-Hrh2, as mentioned before (Fig. S4, c and e). In contrast, the AC activator forskolin blocked the reduction of CREB phosphorylation level rather than the increase in the number of O4$^+$ multipolar differentiating OLs that had been infected with H_2R knockdown virus (AAV-sh-Hrh2) and exposed to OGD (Fig. S4, b, d, and f). These results suggested that the action of H_2R on OL differentiation was independent of the canonical AC/cAMP/CREB pathway.

To further investigate the molecular mechanism underlying the H_2R regulation of OL differentiation, we purified protein complexes and identified protein interactions using the tandem affinity purification method (Xu et al., 2010), combining mass-spectrometric analysis of H_2R binding proteins. The results showed that H_2R may interact with Axin2, which is a negative regulator of the Wnt/β-catenin signaling pathway, by promoting β-catenin degradation. The Wnt/β-catenin signaling pathway has been shown to inhibit OL differentiation (Fancy et al., 2011; Ye et al., 2009). Thus, we speculated that H_2R regulates OL differentiation in an Axin2-related manner. To test this hypothesis, we first verified the interaction between H_2R and Axin2 by coimmunoprecipitation analysis. The result showed that the interaction between H_2R and Axin2 only existed in the context of OGD (Fig. 4 a). We then investigated the effect of H_2R on the Wnt/β-catenin signaling pathway after OGD. We observed that overexpression of H_2R further up-regulated OGD-induced β-catenin expression, which can be significantly counteracted by H_2R knockdown in oli-neu cells (Fig. 4 b). Simultaneously, phosphorylation of GSK3β (p-GSK3β), which is a component of the β-catenin degradation complex (Behrens et al., 1998; Hart et al., 1998), was further decreased by H_2R overexpression in OGD-treated oli-neu cells, while H_2R knockdown increased OGD-induced p-GSK3β (Fig. 4 c). Moreover, total GSK3β had not been regulated by H_2R in the context of OGD (Fig. 4 d). It suggests that H_2R regulates the Wnt/β-catenin signaling pathway following OGD.

To identify the association of H_2R with Axin2 in the Wnt/β-catenin signaling pathway, we used a plasmid to simultaneously overexpress or knock down H_2R and Axin2. We found that cooverexpression of H_2R and Axin2 had no effect on oli-neu cells without OGD exposure, compared with single overexpression of H_2R (Fig. 4 e). However, β-catenin expression was significantly decreased after cooverexpression of H_2R and Axin2 (Flag-Hrh2 plasmid cotransfected with GFP-Axin2 plasmid) in cells that received OGD exposure (Fig. 4 e). This cooverexpression also increased the number of O4$^+$ multipolar differentiating OLs following OGD (Fig. 4 g). These data suggest that the inhibitory effect of H_2R on OL differentiation can be rescued by overexpression of Axin2. Conversely, cotransfection of si-Hrh2 and si-Axin2 to simultaneously interfere with the expression of H_2R and Axin2 increased β-catenin expression and reduced the number of O4$^+$ multipolar differentiating OLs compared with the si-Hrh2 single transfection (Fig. 4, f and h). These results indicate that H_2R negatively regulates OL differentiation through binding with Axin2 to activate the Wnt/β-catenin signaling pathway.

H_2R antagonists accelerate OL differentiation to alleviate the WMI in neonatal HI mice

Although we found that the deletion of H_2R expression promotes remyelination by accelerating OL differentiation, we questioned whether H_2R antagonists could benefit remyelination and functional recovery following neonatal HI WMI. We found that administration of H_2R antagonists cimetidine or zolantidine significantly enhanced the MBP expression in neonatal mice at 28 d, but not at 7 d after HI exposure, suggesting promotion of remyelination (Fig. 5, a1, a2, a5, and b), which was abrogated by H_2R agonist amthamine. In addition, H_2R antagonists had no effect on the increased number of NG2$^+$ OPCs in the corpus callosum at 7 d after HI, but increased O4$^+$ differentiating OLs at 14 d, confirming an improvement in OL differentiation, which can be reversed by amthamine (Fig. 5, a1, a3, and a4).

Our findings demonstrate that H_2R inhibits OL differentiation through the Wnt/β-catenin signaling pathway (Fig. 4). Thus, the Wnt/β-catenin signaling pathway was investigated after H_2R antagonist treatment. We observed that treatment of cimetidine or zolantidine reduced β-catenin expression but elevated p-GSK3β in the corpus callosum following neonatal HI injury, which can be significantly reversed by the combination of amthamine administration (Fig. 5, c and d). Total GSK3β was not regulated by H_2R antagonists in the context of HI (Fig. 5 e). These data suggest that H_2R antagonists promote OL differentiation through down-regulation of the Wnt/β-catenin signaling pathway.

H_2R antagonist cimetidine elevated the percentage of myelinated axons with thicker sheaths (i.e., decreased g-ratio) compared with the HI group, which can be reversed by amthamine (Fig. 5, f1–f3). However, the myelin sheaths in the cimetidine group were still thinner than that in the sham group, indicating remyelinated sheaths (i.e., increased g-ratio). A

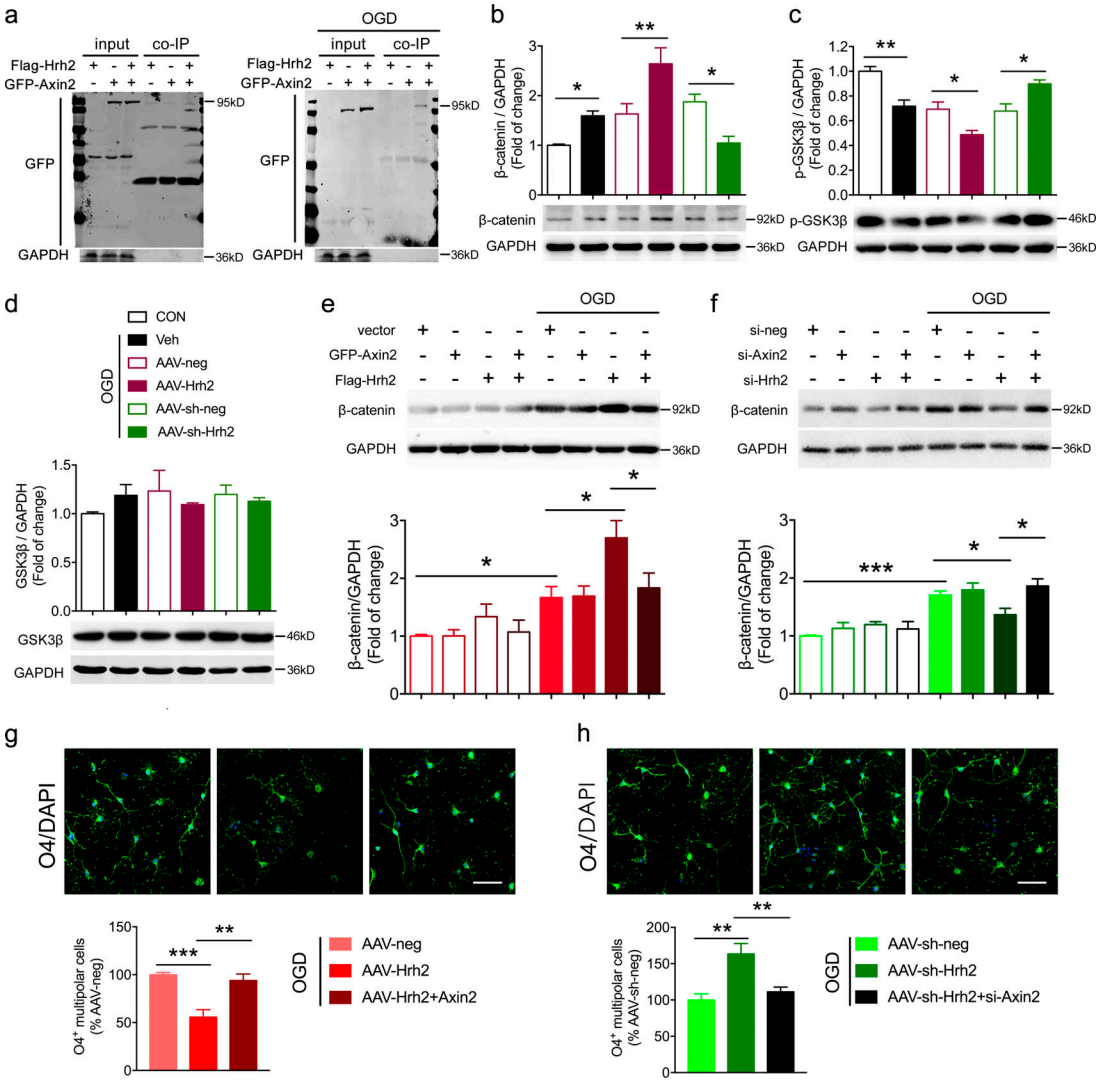

Figure 4. **H_2R inhibits OL differentiation by binding with axin2 to up-regulate the Wnt/β-catenin signaling pathway. (a)** Representative co-immunoprecipitation results showing the interaction of H_2R with Axin2 following OGD/reperfusion (bands of GFP are located at ~95 kD). **(b–d)** Western blot analysis showing the effect of H_2R overexpression (AAV-Hrh2) or knockdown (AAV-sh-Hrh2) on β-catenin, p-GSK3β, and GSK3β expression in OGD-treated oli-neu cells. **(e)** Western blot analysis showing the effect of Flag-Hrh2 plasmid cotransfection with GFP-Axin2 plasmid on β-catenin expression compared with the Flag-Hrh2 single transfection in OGD-treated oli-neu cells. **(f)** Western blot analysis showing the effect of small interfering (si)-Hrh2 cotransfection with si-Axin2 on β-catenin expression compared with the si-Hrh2 single transfection in OGD-treated oli-neu cells. **(g and h)** Immunocytochemical visualization and quantification of primary $O4^+$ multipolar differentiating OLs that received the transfection of AAV-Hrh2 and Axin2 plasmid (g) or transfection of AAV-sh-Hrh2 and si-Axin2 (h) and exposure to OGD/reperfusion. *n* = 4–7 from at least three independent experiments. Scale bar, 50 µm. *, P < 0.05; **, P < 0.01; ***, P < 0.001. co-IP, co-immunoprecipitation; CON, control; Veh, vehicle.

fluorescent cholera toxin B subunit (CTB555) was injected into the primary somatosensory barrel cortex to retrogradely trace axonal projections. We found that the number of CTB555-labeled neurons in the contralateral cortex was reduced at 28 d after HI, indicating the disruption of cortico-cortical axonal connectivity (Fig. 5 g). Treatment of the H_2R antagonist cimetidine significantly increased the number of CTB555-labeled neurons, suggesting improved cortico-cortical axonal connectivity, which was abrogated by the H_2R agonist amthamine.

H_2R antagonists also alleviated the impairment of cognition and motor coordination in rotarod, object recognition, and Morris water maze tests following the exposure to HI (Fig. 5, h, i, and j1–j4). This protection provided by H_2R antagonists can be completely reversed by the H_2R agonist amthamine. These observations suggest that H_2R antagonists may be potential candidates for myelin repair and functional recovery in the neonatal HI WMI. To confirm that the functional benefits provided by H_2R antagonists result from their direct actions on the OL lineage, we observed the effect of cimetidine after the overexpression of H_2R in OLs in a two-site LPC injection model that induces myelin injury as well as functional deficits (Luo et al., 2018). The results showed that LPC induced the impairments in motor coordination and cognitive abilities evaluated by rotarod and object recognition tests, along with the myelin injury in corpus callosum (Fig. S3, b1–b4). H_2R antagonist cimetidine significantly reduced the demyelinated area and improved the

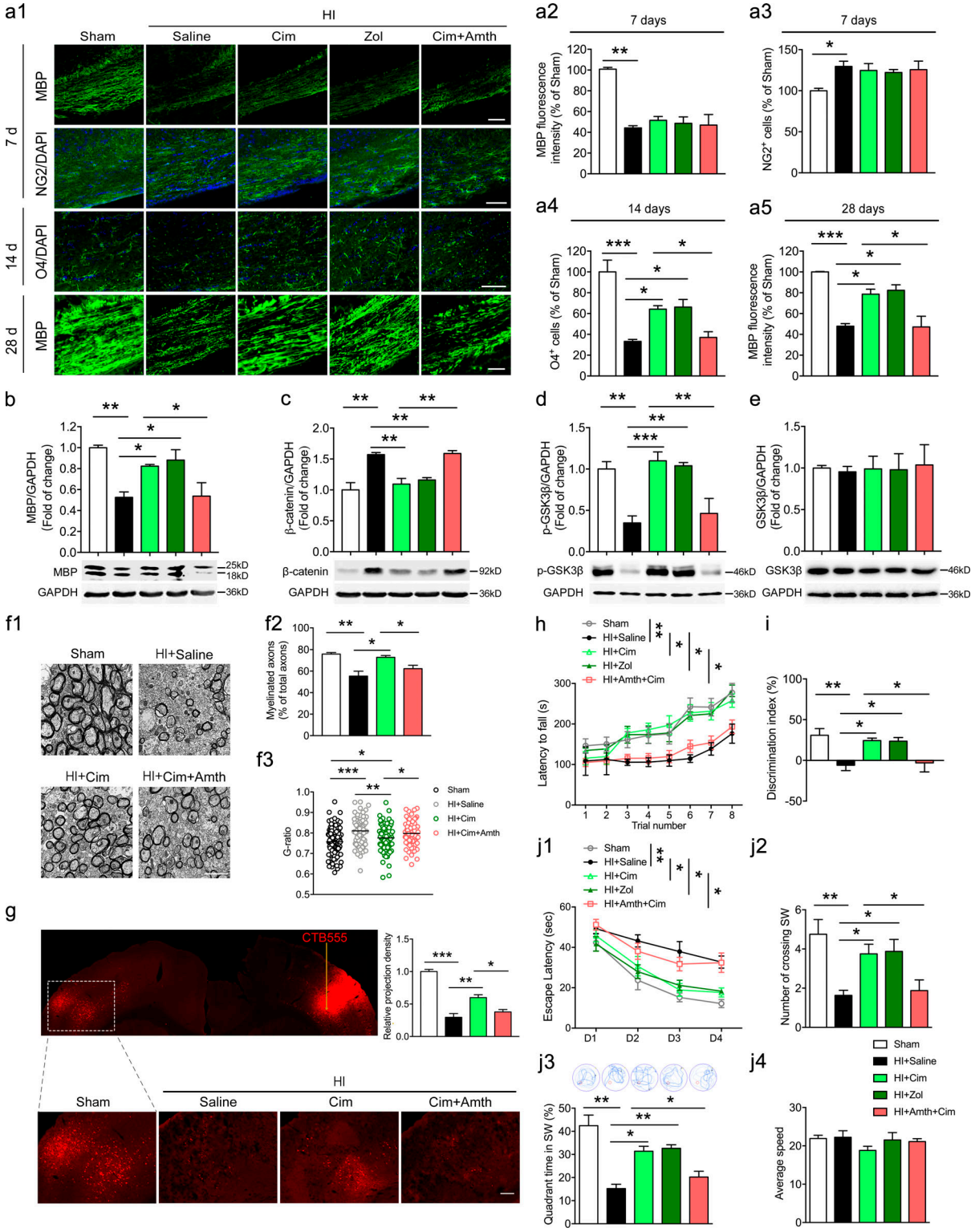

Figure 5. **H_2R antagonists accelerate OL differentiation to alleviate the WMI and neurological function impairments in neonatal HI mice.** Neonatal mice were subjected to unilateral common carotid artery ligation plus inhalational hypoxia and administrated with H_2R antagonist cimetidine (Cim) or zolantidine (Zol), or cimetidine combined with H_2R agonist amthamine (Amth) from 1 d to 28 d after HI. **(a1–a5)** Immunohistochemical visualization and quantification of MBP expression and $NG2^+$ OPC numbers at 7 d, $O4^+$ differentiating OL numbers at 14 d, and MBP expression at 28 d after HI surgery in the corpus callosum of mice administrated with H_2R antagonists or agonists. *n* = 3–5 mice for each group from at least three independent experiments. All scale bars, 100 µm. **(b–e)** Western blot analysis of MBP expression at 28 d, as well as β-catenin, p-GSK3β, and GSK3β expression at 14 d after HI. *n* = 3–5 mice for each group from at least three independent experiments. **(f1–f3)** Representative images, the percentage of myelinated axon fibers, and the g-ratio of myelinated axons in the corpus callosum from electron microscopy at 28 d after HI. *n* = 3 mice for each group from at least two independent experiments in f1 and f2; *n* = 71–104 axons for each group from three mice in f3. Scale bar, 2 µm. **(g)** CTB555 was injected into the primary somatosensory barrel cortex to

retrogradely trace axonal projections. The fluorescence-labeled neurons in the contralateral cortex were quantified. *n* = 6 mice for each group from three independent experiments. **(h)** Motor coordination evaluated by latency to fall from a rotating cylinder at 28 d after neonatal HI in mice administered H_2R antagonists or agonist. **(i and j1–j4)** Cognitive behavior was evaluated by discrimination index in object recognition test (i) and Morris water maze test (j1–j4) from 28 d to 35 d after HI in mice administered H_2R antagonists or agonist. **(j1)** Latency to reach the platform during the acquisition trial. **(j2)** Crossing number and (j3) searching time in the quadrant SW (target quadrant) in the probe trial. **(j4)** Average speed in the probe trial. *n* = 8–10 mice for each group from at least three independent behavior experiments. *, P < 0.05; **, P < 0.01; ***, P < 0.001.

motor coordination and cognitive abilities, while these protective effects were abrogated by overexpression of H_2R in OLs through the injection of AAV-FLEX-Hrh2 into the corpus callosum of *CNPase-Cre* mice. It suggests that H_2R antagonists provide functional protection through their direct actions on the OL lineage.

To study whether the effect of H_2 antagonist cimetidine is histamine-dependent, we employed mice with knockout mutation of the *HDC* gene to block the synthesis of histamine (Fig. S3 e). We found that $HDC^{-/-}$ mice showed comparable size of demyelinated area as controls after LPC injections, while cimetidine still reduced the size of demyelinated area in $HDC^{-/-}$ mice. It suggests that the effect of H_2R antagonist cimetidine on remyelination might be histamine-independent. The coimmunoprecipitation analysis was performed to detect the interaction of H_2R with Axin2 after H_2R ligand treatment and OGD exposure (Fig. S5 a). The results showed that histamine had no effect on the interaction of H_2R with Axin2; however, cimetidine reduced their interaction, which can be reversed by amthamine. It implies that the interaction of H_2R with Axin2 was present and reached saturation after OGD, which can be dismissed by blocking H_2R.

Since WMIs are often identified months after birth, different treatment regimens of H_2R antagonists were employed (Fig. S5, c1–c3 and d1–d3). The results showed that either the delayed (7–35 d after the surgery) or shortened (7–28 d after the surgery) administration of H_2R antagonist cimetidine also enhanced the MBP expression and the number of $O4^+$ differentiating OLs following neonatal HI, which was comparable to that in regular treatment (1–28 d after the surgery; Fig. 5, a4 and a5). All the above effects induced by cimetidine were reversed by the H_2R agonist amthamine.

Discussion

Differentiating OLs are the predominant cell lineage present in human cerebral white matter at the neonatal stage, which could serve as the source for producing myelin through the differentiation into mature OLs (Deng, 2010). This differentiation is largely impeded following neonatal HI, leading to the deficiency of remyelination and neurological recovery (Back et al., 2002; Khwaja and Volpe, 2008). This work validated the expression of H_2R in OLs at all stages and demonstrated that the H_2R in OLs is an important rate-limiting modulator for their differentiation and axonal remyelination in HI-induced neonatal WMI by using AAV-mediated knockdown or overexpression and $Hrh2^{fl/fl}$;*CNPase-Cre* mice in multiple in vivo and in vitro WMI models.

Several features of the action of H_2R on OL differentiation have been identified. First, H_2R inhibits OL differentiation in pathological conditions, such as HI, but not during development. $Hrh2^{fl/fl}$;*CNPase-Cre* mice exhibited comparable white matter microstructure to $Hrh2^{fl/fl}$ mice without exposure to HI (Fig. 3), and overexpression or knockdown of H_2R had no effect on the differentiation of OLs that have not been exposed to OGD (Fig. S2, h1–h3 and i). This could be because the interaction between H_2R and Axin2 and their regulation of the Wnt/β-catenin signaling pathway were only present after pathological insults, such as the OGD (Fig. 4, a, e, and f). So pathological insults, such as the ischemia/OGD and LPC, are primary requirements for the negative regulation by H_2R of OL differentiation. Second, H_2R only played a significant role in OLs undergoing differentiation, without affecting the OL at the OPC stage or mature stage. We found that knockdown or overexpression of H_2R had no effect on the OPC or mature OL pool following OGD (Fig. 1, a1–a3, e1, and e2). However, H_2R negatively regulated the differentiation of preOLs or immature OLs, but not the initiation of differentiation from OPCs (Fig. 1, b1, b2, c1–c3, and d1–d5). Moreover, neither deletion of H_2R in differentiating OLs nor treatment of H_2R antagonists altered the OPC pool or prevented demyelination in neonatal HI mice (Fig. 3, a1–a3; and Fig. 5, a1–a3). Third, H_2R decelerates the OL differentiation process to impede the remyelination. We found that knockdown of H_2R recovered the decreased OL differentiation rate after OGD without affecting their survival or apoptosis (Fig. 1, f1–f3; and Fig. S2, e1, e2, f, and g). Moreover, deletion of H_2R in OLs had no effect on the OPC proliferation or survival of OL lineage, but increased the differentiating OL numbers and promoted the remyelination (Fig. 2, b–m; and Fig. 3, a1–a5). Fourth, H_2R inhibits OL differentiation through the binding with Axin2 and regulating Wnt/β-catenin signaling pathway rather than the canonical AC/cAMP/CREB downstream cascade (Fig. 4 and Fig. S4). Although H_2R in OLs was also found to modulate the AC/cAMP/CREB pathway, this pathway seems not be involved in the regulation of OL differentiation. This could be the reason for the distinctive effects on the differentiation of other cell types conferred by H_2R, which promotes differentiation in neural stem cells and promonocytic cell lines (Molina-Hernández and Velasco, 2008; Monczor et al., 2006). H_2R negatively regulating OL differentiation could be viewed as a novel pathological mechanism in neonatal WMI induced by HI, and could serve as a new component of the current theory of the functional role of H_2R, based on its mostly unknown actions in the brain.

Neonatal HIE produces a complex and heterogeneous injury to the developing brain; however, the characteristic pathological alteration includes WMI, which leads to lifelong cognitive and neurobehavioral dysfunction. Since neural structures are still developing and connections are still being formed at birth, the application of drugs should be carefully considered at this stage.

There are currently no proven treatments for neonatal HIE, other than hypothermia treatment and supportive care (Douglas-Escobar and Weiss, 2015; Yildiz et al., 2017). Previous studies screening remyelination compounds have yielded a number of potent candidates that can increase oligodendroglial differentiation. Clemastine, a muscarinic receptor and histamine H_1 receptor antagonist, and (±)U50488, a kappa opioid receptor agonist, are two such candidates. Clemastine is effective for remyelination in multiple sclerosis patients by blocking M receptor, and recently both clemastine and (±)U50488 were found to promote OL differentiation and functional recovery in neonatal hypoxic brain injury in mice (Cree et al., 2018; Mei et al., 2016; Wang et al., 2018). However, undesirable side effects such as sedation, dysphoria, or hallucinogenic effects due to blocking these receptors may dampen the therapeutic potential of these agents (Simons, 2002; Simons and Simons, 2008). H_2R antagonists with a favorable safety profile have been used to alleviate gastroesophageal reflux disease in extremely preterm infants and full-term infants (Slaughter et al., 2016). Thus, our study strongly suggests that the H_2R in OLs is an effective and reliable therapeutic target for HIE, considering its robust action on remyelination but no effect on physical myelin development, as well as the present application of H_2R antagonists in infants. Moreover, the H_2R in astrocytes or microglia showed no action on the remyelination (Fig. S3, c1, c2, d1, and d2; and Fig. S5, b1 and b2), further supporting the H_2R in OLs viewed as a specific therapeutic target for HIE. H_2R antagonists may be potential candidates for the treatment of HIE, since peripheral H_2R antagonist treatment accelerated OL differentiation by acting on the Wnt/β-catenin signaling pathway to benefit remyelination and alleviate the impairment of axonal connectivity, cognition, and motor coordination in neonatal mice exposed to HI. Treatment with H_2R antagonists seems feasible since the therapeutic regimen can be shortened and delayed until an age that is comparable to months after birth in humans with respect to the myelin development (Jakovcevski et al., 2009), when WMI can be detected by magnetic resonance imaging. Interestingly, activation of H_2R provides neuroprotection from ischemic stroke that is caused by a sudden vascular occlusion and usually induces neuronal damage in a localized cerebral region followed by neuroinflammation and glial scar formation (Hu and Chen, 2017). Activation of H_2R may alleviate neuronal excitotoxicity and inflammatory cell infiltration at an early stage, as well as facilitate astrocyte migration toward the infarct core to inhibit glial scar in the ischemic cerebral injury (Dai et al., 2006; Hiraga et al., 2007; Liao et al., 2015). The discrepancy for the actions of H_2R suggests the role of H_2R in ischemia may depend on the cell type or ischemia type. H_2R antagonists may be applicable to the therapy for WMI induced by HI, but not the ischemic stroke.

In conclusion, our results demonstrated that H_2R negatively regulates differentiation in OLs following neonatal HI through binding with Axin2 and subsequently modulation of Wnt/β-catenin signaling pathway. Our results suggest that the H_2R in OLs could serve as an effective and secure therapeutic target for the retard of OL differentiation and remyelination in the pathological progress of neonatal HIE. The H_2R antagonists that have been used for gastroesophageal reflux in preterm and full-term infants may have potential therapeutic value for neonatal HIE.

Materials and methods

Animal experiments

All experiments and protocols were approved by and conducted in accordance with the ethical guidelines of the Zhejiang University Animal Experimentation Committee and were in complete compliance with the National Institutes of Health Guide for the Care and Use of Laboratory Animals. Efforts were made to minimize any pain or discomfort, and the minimum number of animals was used. Neonatal HI was induced in C57BL/6 mice at P7-9, as described by Skoff et al. (2001). Pups of either sex were anesthetized with isoflurane (3.0% for induction, 1.0% for maintenance) in oxygen gas, and the right common carotid artery was isolated and ligated with 8/0 surgical silk. The procedure was completed within 5 min. After this procedure, the pups recovered for 2 h in a temperature-controlled incubator. The pups were then placed in a chamber perfused with a humidified gas mixture (8% oxygen in nitrogen) for 50 min hypoxia. The temperature in the incubator was kept at 36°C.

To create the focal demyelination model (Fancy et al., 2011), 8–10 wk old C57BL/6 mice were anesthetized by intraperitoneal injection of sodium pentobarbital (50 mg/kg) and mounted on a stereotaxic frame (RWD Life Science). 1 µl of 1% LPC (Sigma-Aldrich) in 0.9% NaCl was microinjected into the corpus callosum (anteroposterior [AP], +1.0 mm; mediolateral [ML], −0.9 mm; dorsoventral [DV], −2.2 mm) using precision glass syringes (Hamilton Company). In a two-site LPC injection model, LPC was microinjected into the corpus callosum (AP, +0.8 mm; ML ±1.0 mm; DV, −2.2 mm) using precision glass syringes (Hamilton Company). Each site was injected with 1 µl of 1% LPC (Sigma-Aldrich) in 0.9% NaCl within 10 min (Luo et al., 2018). The day of LPC injection was designated day 0 (0 dpl). Mice in the sham group were injected with 1 µl of saline. In the LPC-induced demyelination model, 600 nl virus was injected at 3 wk before the LPC injection.

Hrh2$^{fl/fl}$ mice were generated by standard homologous recombination at the Nan Jing Biomedical Research Institute of Nanjing University (Nanjing, China). Exon 2 encoding the core region of Hrh2 was flanked on either side by loxP sequences. To specifically delete *Hrh2* in differentiating OLs, *Hrh2*$^{fl/fl}$ homozygous mice were mated with *CNPase-Cre* mice (provided by D. Shuming, Zhejiang University, Hangzhou, China) to generate *Hrh2*$^{fl/fl}$*;CNPase-Cre* mice. The genetic background of all mouse strains is C57BL/6. Only male offspring were used for experiments. For genotyping of *Hrh2*$^{fl/fl}$ mice, two pairs of oligos were used. For the primer pair of Hrh2-loxp-tF, 5′-CTTGTGGAGGTG ATCTGGTGA-3′ and Hrh2-loxp-tR, 5′-CGCCCATGTCTAAGCGTT AT-3′, the PCR products were 417 bp (floxed allele) and 299 bp (wild-type allele). For genotyping of *CNPase-Cre* mice, one pair of oligos, cnp-cre-tF, 5′-GATGGGGCTTACTCTTGC-3′ and cnp-cre-tR, 5′-CATAGCCTGAAGAACGAGA-3′, was used, and the PCR products were 894 bp (mutated allele).

To investigate whether H_2R in microglia or astrocytes was also involved in remyelination, we selectively overexpressed

H_2R in microglia by injection of a Cre-dependent lentivirus, pSLenti-PGK-FLEX-Hrh2 (Lenti-FLEX-Hrh2), into the corpus callosum of *CX3CR1-CreER* mice (Jackson Laboratory), or overexpressed or knocked down H_2R in astrocytes by injection of AAV-FLEX-Hrh2 or AAV-FLEX-sh-Hrh2 in *GFAP-Cre* mice (Jackson Laboratory). The genetic background of all mouse strains is C57BL/6. For genotyping of *GFAP-Cre* mice, one pair of oligos, gfap-cre-tF, 5′-GCGGTCTGGCAGTAAAAACTATC-3′ and gfap-cre-tR, 5′-GTGAAACAGCATTGCTGTCACTT-3′, was used, and the PCR products were 100 bp (mutated allele). For genotyping of *CX3CR1-Cre* mice, one pair of oligos, cx3cr1-cre-tF, 5′-AAGACTCACGTGGACCTGCT-3′ and cx3cr1-cre-tR, 5′-CGGTTATTCAACTTGCACCA-3′, was used, and the PCR products were 300 bp (mutated allele).

To investigate whether the effect of H_2R in remyelination was ligand independent, the $HDC^{-/-}$ mice (provided by H. Ohtsu, Tohoku University, Sendai, Japan) were intraperitoneally administrated with H_2R antagonist cimetidine (20 mg/kg/d; Sigma-Aldrich) after LPC microinjection. The genetic background of $HDC^{-/-}$ mice is C57BL/6. For genotyping of $HDC^{-/-}$ mice, one pair of oligos, hdc-tF, 5′-AAACATCGCATCGAGCGAGCACGTACTCGG-3′ and hdc-tR, 5′-ATGTCCTGATAGCGGTCCGCCACACCCAGC-3′, was used, and the PCR products were 244 bp (mutated allele). $HDC^{-/-}$ mice were fed with special chow low in histamine (0.5 µg/g).

Cell cultures

Purified OPCs were isolated using the shake off method as previously described (Shi et al., 2018; Zhou et al., 2014, 2017). Briefly, mixed cortical glial cells generated from postnatal day (P0) rats were cultured in DMEM (Invitrogen) supplemented with 15% FBS (Biological Industries) for 10–12 d at 37°C under 5% CO_2; the medium was changed every 3 d. The culture flasks were shaken at 200 rpm for 1 h followed by an additional 16 h at 250 rpm with fresh medium at 37°C. The cell suspension was subcultured in uncoated dishes for 1 h at 37°C under 5% CO_2. It allowed the astrocytes and microglia to firmly attach to the dishes, whereas the OPCs could be collected with gentle shaking of the dishes. Collected OPCs were then subcultured onto poly-L-lysine–coated plates, dishes, or coverslips and maintained in neurobasal medium supplemented with 2% B27 (Invitrogen), 10 ng/ml basic fibroblast growth factor, and 10 ng/ml PDGF-AA (PeproTech) to keep them undifferentiated (Yang et al., 2005). PDGF-AA and basic fibroblast growth factor were excluded from the OPC medium, and 3,3′,5-triiodo-L-thyronine (T3; 40 ng/ml; Sigma-Aldrich) and ciliary neurotrophic factor (CNTF; 10 ng/ml; Sigma-Aldrich) were added to allow their differentiation into preOLs, immature OLs, or mature OLs. The purity of $Olig2^+$ OLs, $NG2^+$ OPCs, or $O4^+$ differentiating preOLs was confirmed by immunostaining (Fig. S2 a).

The immortalized mouse oligodendrocytic cell line oli-neu was provided by Q. Weng (Zhejiang University, Hangzhou, China) with permission from Q.R. Lu (University of Cincinnati, Cincinnati, OH). Oli-neu cells were grown in DMEM medium containing 5% FBS, 1% horse serum (Biological Industries), 2% B27, and 1% N-2 Supplement (Invitrogen) and differentiated in T3 (40 ng/ml; Sigma-Aldrich) and CNTF (10 ng/ml; Sigma-Aldrich) with added DMEM.

For OGD exposure, cells were refreshed with O_2- and glucose-free DMEM, and immediately placed in a sealed chamber (Billups-Rothenburg) loaded with mixed gas containing 5% CO_2 and 95% N_2. Cells were exposed to OGD for 2 h and refreshed with normal culture medium for 24 h.

Drug administration

Mice were intraperitoneally injected with saline, H_2R antagonist cimetidine (20 mg/kg/d; Sigma-Aldrich), zolantidine (10 mg/kg/d; Sigma-Aldrich), or cimetidine combined with H_2R agonist amthamine (5 mg/kg/d; Sigma-Aldrich) after neonatal HI surgery. Mice were intraperitoneally injected with saline or H_2R antagonist cimetidine (20 mg/kg/d; Sigma-Aldrich) after LPC microinjection in a two-site LPC injection model.

AAV-sh-Hrh2– or AAV-Hrh2–infected oli-neu cells or primary cultured OLs were treated with forskolin (100 nM) or SQ22536 (100 µM) during reperfusion

Cultured human embryonic kidney (HEK) 293 cells transfected with Flag-H_2R and GFP-Axin2 plasmids were exposed to 2 h OGD and 24 h reperfusion with normal culture medium. To investigate whether interaction of H_2R with Axin2 was ligand-independent, histamine (10 µM; Sigma-Aldrich), cimetidine (10 µM; Sigma-Aldrich) or cimetidine combined with amthamine (10 µM; Sigma-Aldrich) was added in HEK 293 cells during reperfusion of OGD.

Virus infection and retrograde axonal tracer injection

AAV-Hrh2-mCherry (AAV-Hrh2), AAV-neg-mCherry (AAV-neg, control virus), AAV-sh-Hrh2-mCherry (AAV-sh-Hrh2), AAV-sh-neg-mCherry (AAV-sh-neg, control virus), AAV-CAG-FLEX-Hrh2-GFP (AAV-FLEX-Hrh2), AAV-CAG-FLEX-sh-Hrh2-GFP (AAV-FLEX-sh-Hrh2), AAV-CAG-FLEX-GFP (AAV-FLEX-neg, control virus), pSlenti-PGK-FLEX-Hrh2 (Lenti-FLEX-Hrh2), and pSlenti-PGK-FLEX-GFP (Lenti-FLEX-neg, control virus) were produced by OBiO Technology to overexpress, knock down, or Cre-dependently overexpress H_2R. The sequence for the *Hrh2* shRNA was 5′-GATCCCCGCAGGTCAACGAGGTATATGGCTCGAGCCATATACCTCGTTGACCTGCTTTTT-3′. The sequence for the control shRNA was 5′-GATCCCCTTCTCCGAACGTGTCACGTTTCAAGAGAACGTGACACGTTCGGAGAATTTTTTGTAC-3′. Mice at 8–10 wk old were placed in a stereotaxic apparatus (RWD Life Science) after anesthesia by sodium pentobarbital (50 mg/kg, i.p.). AAV-Hrh2, AAV-sh-Hrh2, AAV-FLEX-Hrh2, AAV-FLEX-sh-Hrh2, or Lenti-FLEX-Hrh2 or the control viruses were injected into the corpus callosum (600 nl, 10 min; AP +1.0 mm, ML −0.9 mm, and DV −2.2 mm). In a two-site LPC injection model, AAV-FLEX-Hrh2 or AAV-FLEX-neg was injected into the corpus callosum (600 nl, 10 min; AP +0.8 mm, ML ±1.0 mm, and DV −2.2 mm) before LPC injection. Mice were kept in the home cage for 3 wk to allow virus expression, which was checked by GFP or mCherry expression in the targeted region. Only mice with the correct locations of viral expression were used for further analysis. For infection in cells, AAV-Hrh2, AAV-sh-Hrh2, or their control virus was added to cells in culture medium for 24 h.

A fluorescent CTB555 (200 nl, 10 min) was injected into the primary somatosensory barrel cortex at 14 d after HI surgery to retrogradely trace axonal projections. Mice were perfused transcardially with 4% paraformaldehyde (PFA) in PBS (pH 7.4). Frozen brain sections of 20 µm were obtained using a cryostat (SM2000R, Leica). Fluorescent images were taken using Leica SP8 laser confocal microscope. The fluorescence labeled neurons in the contralateral cortex was quantified by ImageJ software (National Institutes of Health) and normalized to the sham group.

Electroporation

Primary cultured OLs were transfected with GFP-Axin2 plasmids or si-Axin2 by the Amaxa Rat Oligodendrocyte Nucleofection Kit (Lonza) according to the manufacturer's instructions. Briefly, 5 × 10^6 cells were collected during culture of primary OLs and then resuspended with 100 µl Nucleofector solution containing 3 µg DNA or 200 pmol siRNA duplexes. The cell suspension was transferred into a cuvette and electroporated with Nucleofector program O-17.

Behavior assays

Accelerating rotarod

The rotarod apparatus was set to accelerate from 5 to 40 rpm in 300 s, and mice were placed in separate lanes on the rod, which was initially rotating at 5 rpm. The trial began when acceleration started and ended when mice fell off the rod. If a mouse clung to the rod and completed a full passive rotation, the timer was stopped. Each mouse was assessed over eight trials with 20-min intertrial intervals.

Novel object recognition test

As reported before (Ma et al., 2015), this task was conducted in an open field box with two different kinds of objects. During habituation, the mice were allowed to explore an open field box for 10 min. 24 h after habituation, the mice were exposed to the familiar box with two identical objects placed at an equal distance for 10 min. After a 30-min intertrial interval, one of the objects presented in the first trial was replaced with a new object, and the mice were allowed to explore for 3 min. Exploration was recorded when mice directed the nose at a distance <1 cm from the object and/or touched it with the nose. The exploration time spent on each of the familiar (*F*) objects and the new (*N*) object was recorded manually in a blind manner. The discrimination index percentage was calculated by $(N - F) / (N + F) \times 100\%$ for intergroup comparisons.

Morris water maze test

As reported before (Zhou et al., 2017), a circular pool was filled with water and painted white. The pool was divided into four quadrants (northeast, northwest, southwest [SW], and southeast). A hidden platform (10 cm in diameter) was submerged 1 cm below the water surface in the center of the SW quadrant (target quadrant). Spatial cues consisting of black-and-white posters were constantly visible from the pool. The subjects were monitored by a video tracking system directly above the water tank as they swam. At the acquisition phase, each mouse was trained using four trials per day for 4 d consecutively; the interval between the trials was 10 min. During each trial, the escape latency as the time to reach the platform and climb up out of the water was recorded, but limited to 60 s. On the fifth day, the platform was removed, and the mice were allowed to swim freely for 60 s. The number of platform area crossings and time spent in the target quadrant were recorded.

Immunofluorescent staining

Mice were perfused transcardially with 4% PFA in PBS (pH 7.4). Frozen brain sections of 20 µm were obtained using a cryostat (SM2000R, Leica). Sections were then permeabilizated with 0.5% Triton X-100 for 15 min. Cells were fixed with 4% PFA for 20 min and then permeabilized with 0.1% Triton X-100 for 5 min. Sections or cells were blocked with donkey serum for 2 h and incubated overnight at 4°C with primary antibodies. The next day, sections were incubated with secondary antibodies for 2 h at room temperature. Primary antibodies included the following: rabbit anti-H_2R (1:200, Abcam); rat anti-H_2R (1:100, Alomone Labs); rat anti-MBP (1:250, Millipore); rabbit anti-Olig2 (1:500, Millipore); rabbit anti-NG2 (1:300, Abcam); goat anti-PDGFRα (1:30, R&D Systems); rabbit anti-CNP (1:400, Abcam); mouse anti-O4 (1:150, Millipore); mouse anti-CC-1 (1:400, Abcam); rabbit anti-Ki67 (1:200, Abcam); mouse anti-NF200 (1:100, Abcam); rabbit anti-Iba-1 (1:200, Abcam); and rabbit anti-GFAP (1:400, Lianke). Secondary antibodies included the following: Alexa Fluor 488 secondary antibodies or Alexa Fluor 594 secondary antibodies to rabbit, rat, mouse, chicken, or goat (1:400, Jackson ImmunoResearch). Nuclei were counterstained with DAPI. Apoptotic cells were determined using a TUNEL assay (Yeasen) according to the manufacturer's protocol before the incubation of primary antibodies. Fluorescent images were taken using an Olympus FV1000 or Leica SP8 laser confocal microscope. The fluorescence intensity analysis and cell counting were performed using ImageJ software (National Institutes of Health) in the ipsilateral corpus callosum at similar coronal positions of each animal or in at least three coverslips from each group.

In situ hybridization

Frozen brain slices with 14-µm thickness mounted on adhesion microscope slides (CITOGLAS) were subjected to in situ hybridization. The mouse *Hrh2* probe and RNAscope 2.5 HD Detection Reagent Kit-Red/RNAscope Multiplex Fluorescent Reagent Kit v2 (Advanced Cell Diagnostics) were used for *Hrh2* expression in OL lineages, microglia, astrocytes, or pericytes, together with immunostaining of NG2, O4, CNP, CC-1, Olig2, Iba-1, GFAP, PDGFRβ, or GFP. RNAscope Multiplex Fluorescent Reagent Kit v2 (Advanced Cell Diagnostics) was used for duplex hybridization by combining the Hrh2 probe C1 with a GFP probe C2 for validation of *Hrh2* reexpression. For combined in situ hybridization and immunofluorescence analyses, the slices were then incubated with rabbit anti-NG2 (1:300, Millipore), mouse anti-O4 (1:150, Millipore), rabbit anti-CNP (1:400, Abcam), mouse anti-CC-1 (1:400, Abcam), rabbit anti-Olig2 (1:500, Millipore), rabbit anti-Iba-1 (1:200, Abcam), rabbit anti-GFAP (1:400, Lianke), goat anti-PDGFRβ (1:20, R&D Systems), or chicken

anti-GFP (1:400, Abcam). Fluorescent images were taken using an Olympus FV1000 or Leica SP8 laser confocal microscope.

Western blot

The corpus callosum of mice was carefully separated and then lysed with homogenization buffer. The cells were homogenized in RIPA buffer. Equal amounts (40 µg) of tissue lysates were separated using SDS-PAGE and transferred onto a nitrocellulose membrane. The membranes were incubated with the following primary antibodies: rabbit anti-H_2R (1:500, Abcam); rat anti-MBP (1:1,000, Millipore); rabbit anti-NG2 (1:1,000, Abcam); mouse anti-CC-1 (1:1,000, Abcam); rabbit β-catenin (1:300, Abcam); rabbit GSK3β (1:1,000, Abcam); rabbit GSK3β (phosphor Y216; 1:1,000, Abcam); rabbit cleaved-caspase3 (1:1,000, Abcam); rabbit CREB (1:500, Abcam); rabbit p-CREB (1:500, Abcam) and mouse anti-GAPDH (1:5,000, Kang-chen). Secondary antibodies conjugated with HRP against rabbit, mouse, or rat IgG (1:3,000, Lianke) were applied. Images were acquired with the Tanon Chemiluminescent Imaging System (Tanon) and analyzed by ImageJ software (National Institutes of Health). The results were expressed as the target protein/GAPDH ratio and then normalized to the values measured in the sham or control groups in vivo and in vitro.

Coimmunoprecipitation

Cultured HEK 293 cells transfected with Flag-H_2R and GFP-Axin2 plasmids were exposed to 2 h OGD and 24 h reperfusion with normal culture medium, and then lysed with homogenization buffer. The coimmunoprecipitation of H_2R and Axin2 was performed based on a previously described method (Yuan et al., 2017). The extracts of 500 µg protein were incubated with nonspecific IgG (2 mg, Abcam) or rabbit anti-Flag (2 mg, Abcam) overnight at 4°C, and then anti-rabbit protein G-agarose (Abcam) for 3 h at 4°C. Four lysis buffer washes were conducted on the precipitates, which were then denatured with SDS sample-loading buffer. Proteins were separated on 12% SDS-PAGE and transferred onto nitrocellulose membranes. Transfer membranes were then blocked with Tris-buffered saline with Tween 20 (TBST) containing 5% nonfat dried milk for 1 h at room temperature, and incubated with primary antibody rabbit anti-H_2R (1:500, Abcam), rat anti-GFP (1:500, Abcam), or mouse anti-GAPDH (1:5,000, Kang-chen). Membranes were incubated with the appropriate secondary antibodies (1:3,000, Lianke) for 2 h. Images were acquired with the Tanon Chemiluminescent Imaging System (Tanon). The lanes marked "input" were loaded with 10% of the starting material used for immunoprecipitation.

ELISA

The histamine level in the corpus callosum were quantified by competitive ELISA. In brief, the tissue was homogenized in 0.1 M perchloric acid at room temperature, and the supernatant was collected after centrifugation. Histamine concentration was determined using histamine ELISA kits (Bertin Pharma) according to the manufacturer's instructions. Absorbance was read at 405 nm on a spectrophotometer (Biotek), and concentration was calculated using an equation generated from a standard curve.

LFB staining

Frozen samples containing LPC lesions were cut at 20 µm by a cryostat. The sections were incubated in 95% ethanol for 5 min and with 0.1% LFB overnight at 56°C, and then differentiated with 0.05% lithium carbonate and 70% ethanol (Zhao et al., 2015). The demyelinated area in the corpus callosum was calculated by blinded independent readers.

Electron microscopy

Mice brains were perfused with a phosphate buffer solution containing 2.5% glutaraldehyde and 4% PFA (pH 7.4). Samples of the middle segment of the corpus callosum ipsilateral to the occluded carotid were obtained and kept in the same buffer for 48 h at 4°C. After that, samples were postfixed in 1% osmium tetroxide, dehydrated in cold ethanol, infiltrated, and embedded in Araldite resin. Sections (90 nm) were collected, placed on grids, and stained with uranyl acetate and lead citrate. The grids were then imaged using a transmission electron microscope, and the percentage of myelinated axons and g-ratio were quantified.

Statistical analysis

All data were collected and analyzed in a blind manner. Data are expressed as means ± SEM. Statistical comparisons between two groups were performed using an unpaired Student's *t* test. Comparisons between three or more groups were performed by one-way ANOVA with Dunnett's or Tukey's post hoc test. For the ratio analysis of MBP^+ cell numbers to $O4^+$ (MBP^-) cell numbers (Fig. 1 f) and Morris water maze tests, two-way ANOVA with Tukey's post hoc tests was performed. For all analyses, the tests were two-sided, and $P < 0.05$ was considered statistically significant. GraphPad Prism 7 software was used for all analyses.

Online supplemental material

Fig. S1 demonstrates the H_2R expression in the OL lineages and in different types of cells in the white matter following neonatal HI. Fig. S2 demonstrates the effect of overexpression and knockdown of H_2R on cultured OLs. Fig. S3 demonstrates the effect of overexpression and knockdown of H_2R on remyelination and neurological function in an LPC-induced demyelination model. Fig. S4 shows the effect of overexpression and knockdown of H_2R on the AC/cAMP/CREB pathway during OL differentiation after OGD insult. Fig. S5 shows the effects of H_2R antagonist on the interaction between H_2R and Axin2 or on the WMI in neonatal HI mice.

Acknowledgments

Thanks for the technical support by the Core Facilities, Zhejiang University School of Medicine.

This work was supported by National Natural Science Foundation of China grants 81722045, 81673405, 81872844, and 81973302, Zhejiang Provincial Natural Science Foundation of China grants LR17H310001 and LY18H310003, and the "Ten thousand plan"-high-level talents special support plan of Zhejiang Province (ZJWR0108003).

Author contributions: L. Jiang and W. Hu designed the study and wrote the manuscript. L. Jiang performed most of the

experiments with the help of L. Cheng; H. Chen carried out most of the behavior experiments with the help of D. An; Y. Zheng and Q. Ma analyzed behavior experiments data in a blind manner. H. Dai, X. Zhang, W. Hu, and Z. Chen designed and interpreted some experiments. L. Cheng, H. Dai, X. Zhang, W. Hu, and Z. Chen edited the manuscript. All authors reviewed and approved the manuscript.

Disclosures: The authors declare no competing interests exist.

Submitted: 24 July 2019
Revised: 19 February 2020
Accepted: 27 April 2020

References

Back, S.A., B.H. Han, N.L. Luo, C.A. Chricton, S. Xanthoudakis, J. Tam, K.L. Arvin, and D.M. Holtzman. 2002. Selective vulnerability of late oligodendrocyte progenitors to hypoxia-ischemia. *J. Neurosci.* 22:455–463. https://doi.org/10.1523/JNEUROSCI.22-02-00455.2002

Behrens, J., B.A. Jerchow, M. Würtele, J. Grimm, C. Asbrand, R. Wirtz, M. Kühl, D. Wedlich, and W. Birchmeier. 1998. Functional interaction of an axin homolog, conductin, with beta-catenin, APC, and GSK3beta. *Science*. 280:596–599. https://doi.org/10.1126/science.280.5363.596

Billiards, S.S., R.L. Haynes, R.D. Folkerth, N.S. Borenstein, F.L. Trachtenberg, D.H. Rowitch, K.L. Ligon, J.J. Volpe, and H.C. Kinney. 2008. Myelin abnormalities without oligodendrocyte loss in periventricular leukomalacia. *Brain Pathol.* 18:153–163. https://doi.org/10.1111/j.1750-3639.2007.00107.x

Blakemore, W.F., and R. Franklin. 2008. Remyelination in experimental models of toxin-induced demyelination. *In* Current Topics in Microbiology and Immunology. M. Rodriguez, editor. Springer-Verlag Berlin, Berlin. pp. 193–212.

Buser, J.R., J. Maire, A. Riddle, X. Gong, T. Nguyen, K. Nelson, N.L. Luo, J. Ren, J. Struve, L.S. Sherman, et al. 2012. Arrested preoligodendrocyte maturation contributes to myelination failure in premature infants. *Ann. Neurol.* 71:93–109. https://doi.org/10.1002/ana.22627

Cree, B.A.C., J. Niu, K.K. Hoi, C. Zhao, S.D. Caganap, R.G. Henry, D.Q. Dao, D.R. Zollinger, F. Mei, Y.A. Shen, et al. 2018. Clemastine rescues myelination defects and promotes functional recovery in hypoxic brain injury. *Brain*. 141:85–98. https://doi.org/10.1093/brain/awx312

Dai, H., Z. Zhang, Y. Zhu, Y. Shen, W. Hu, Y. Huang, J. Luo, H. Timmerman, R. Leurs, and Z. Chen. 2006. Histamine protects against NMDA-induced necrosis in cultured cortical neurons through H receptor/cyclic AMP/protein kinase A and H receptor/GABA release pathways. *J. Neurochem.* 96:1390–1400. https://doi.org/10.1111/j.1471-4159.2005.03633.x

Deng, W. 2010. Neurobiology of injury to the developing brain. *Nat. Rev. Neurol.* 6:328–336. https://doi.org/10.1038/nrneurol.2010.53

Douglas-Escobar, M., and M.D. Weiss. 2015. Hypoxic-ischemic encephalopathy: a review for the clinician. *JAMA Pediatr.* 169:397–403. https://doi.org/10.1001/jamapediatrics.2014.3269

Duncan, I.D., R.L. Marik, A.T. Broman, and M. Heidari. 2017. Thin myelin sheaths as the hallmark of remyelination persist over time and preserve axon function. *Proc. Natl. Acad. Sci. USA*. 114:E9685–E9691. https://doi.org/10.1073/pnas.1714183114

Fancy, S.P., E.P. Harrington, T.J. Yuen, J.C. Silbereis, C. Zhao, S.E. Baranzini, C.C. Bruce, J.J. Otero, E.J. Huang, R. Nusse, et al. 2011. Axin2 as regulatory and therapeutic target in newborn brain injury and remyelination. *Nat. Neurosci.* 14:1009–1016. https://doi.org/10.1038/nn.2855

Fancy, S.P., E.P. Harrington, S.E. Baranzini, J.C. Silbereis, L.R. Shiow, T.J. Yuen, E.J. Huang, S. Lomvardas, and D.H. Rowitch. 2014. Parallel states of pathological Wnt signaling in neonatal brain injury and colon cancer. *Nat. Neurosci.* 17:506–512. https://doi.org/10.1038/nn.3676

Franklin, R.J., and C. Ffrench-Constant. 2008. Remyelination in the CNS: from biology to therapy. *Nat. Rev. Neurosci.* 9:839–855. https://doi.org/10.1038/nrn2480

Franklin, R.J., and S.A. Goldman. 2015. Glia Disease and Repair-Remyelination. *Cold Spring Harb. Perspect. Biol.* 7. a020594. https://doi.org/10.1101/cshperspect.a020594

Haas, H.L., O.A. Sergeeva, and O. Selbach. 2008. Histamine in the nervous system. *Physiol. Rev.* 88:1183–1241. https://doi.org/10.1152/physrev.00043.2007

Hart, M.J., R. de los Santos, I.N. Albert, B. Rubinfeld, and P. Polakis. 1998. Downregulation of beta-catenin by human Axin and its association with the APC tumor suppressor, beta-catenin and GSK3 beta. *Curr. Biol.* 8:573–581. https://doi.org/10.1016/S0960-9822(98)70226-X

Hill, S.J., C.R. Ganellin, H. Timmerman, J.C. Schwartz, N.P. Shankley, J.M. Young, W. Schunack, R. Levi, and H.L. Haas. 1997. International Union of Pharmacology. XIII. Classification of histamine receptors. *Pharmacol. Rev.* 49:253–278.

Hiraga, N., N. Adachi, K. Liu, T. Nagaro, and T. Arai. 2007. Suppression of inflammatory cell recruitment by histamine receptor stimulation in ischemic rat brains. *Eur. J. Pharmacol.* 557:236–244. https://doi.org/10.1016/j.ejphar.2006.11.020

Hu, W., and Z. Chen. 2017. The roles of histamine and its receptor ligands in central nervous system disorders: An update. *Pharmacol. Ther.* 175:116–132. https://doi.org/10.1016/j.pharmthera.2017.02.039

Jakovcevski, I., R. Filipovic, Z. Mo, S. Rakic, and N. Zecevic. 2009. Oligodendrocyte development and the onset of myelination in the human fetal brain. *Front. Neuroanat.* 3:5. https://doi.org/10.3389/neuro.05.005.2009

Khwaja, O., and J.J. Volpe. 2008. Pathogenesis of cerebral white matter injury of prematurity. *Arch. Dis. Child. Fetal Neonatal Ed.* 93:F153–F161. https://doi.org/10.1136/adc.2006.108837

Kurinczuk, J.J., M. White-Koning, and N. Badawi. 2010. Epidemiology of neonatal encephalopathy and hypoxic-ischaemic encephalopathy. *Early Hum. Dev.* 86:329–338. https://doi.org/10.1016/j.earlhumdev.2010.05.010

Liao, R.J., L. Jiang, R.R. Wang, H.W. Zhao, Y. Chen, Y. Li, L. Wang, L.Y. Jie, Y.D. Zhou, X.N. Zhang, et al. 2015. Histidine provides long-term neuroprotection after cerebral ischemia through promoting astrocyte migration. *Sci. Rep.* 5:15356. https://doi.org/10.1038/srep15356

Luo, Q., L. Ding, N. Zhang, Z. Jiang, C. Gao, L. Xue, B. Peng, and G. Wang. 2018. A stable and easily reproducible model of focal white matter demyelination. *J. Neurosci. Methods*. 307:230–239. https://doi.org/10.1016/j.jneumeth.2018.05.024

Ma, J., J. Zhang, W.W. Hou, X.H. Wu, R.J. Liao, Y. Chen, Z. Wang, X.N. Zhang, L.S. Zhang, Y.D. Zhou, et al. 2015. Early treatment of minocycline alleviates white matter and cognitive impairments after chronic cerebral hypoperfusion. *Sci. Rep.* 5:12079. https://doi.org/10.1038/srep12079

Mei, F., S.R. Mayoral, H. Nobuta, F. Wang, C. Desponts, D.S. Lorrain, L. Xiao, A.J. Green, D. Rowitch, J. Whistler, et al. 2016. Identification of the Kappa-Opioid Receptor as a Therapeutic Target for Oligodendrocyte Remyelination. *J. Neurosci.* 36:7925–7935. https://doi.org/10.1523/JNEUROSCI.1493-16.2016

Miu, A.C., R.M. Heilman, S.P. Paşca, C.A. Stefan, F. Spânu, R. Vasiu, A.I. Olteanu, and M. Miclea. 2006. Behavioral effects of corpus callosum transection and environmental enrichment in adult rats. *Behav. Brain Res.* 172:135–144. https://doi.org/10.1016/j.bbr.2006.05.007

Molina-Hernández, A., and I. Velasco. 2008. Histamine induces neural stem cell proliferation and neuronal differentiation by activation of distinct histamine receptors. *J. Neurochem.* 106:706–717. https://doi.org/10.1111/j.1471-4159.2008.05424.x

Monczor, F., N. Fernandez, E. Riveiro, A. Mladovan, A. Baldi, C. Shayo, and C. Davio. 2006. Histamine H2 receptor overexpression induces U937 cell differentiation despite triggered mechanisms to attenuate cAMP signalling. *Biochem. Pharmacol.* 71:1219–1228. https://doi.org/10.1016/j.bcp.2005.12.037

Panula, P., and S. Nuutinen. 2013. The histaminergic network in the brain: basic organization and role in disease. *Nat. Rev. Neurosci.* 14:472–487. https://doi.org/10.1038/nrn3526

Passani, M.B., P. Panula, and J.S. Lin. 2014. Histamine in the brain. *Front. Syst. Neurosci.* 8:64. https://doi.org/10.3389/fnsys.2014.00064

Rajasekharan, S., K.A. Baker, K.E. Horn, A.A. Jarjour, J.P. Antel, and T.E. Kennedy. 2009. Netrin 1 and Dcc regulate oligodendrocyte process branching and membrane extension via Fyn and RhoA. *Development*. 136:415–426. https://doi.org/10.1242/dev.018234

Segovia, K.N., M. McClure, M. Moravec, N.L. Luo, Y. Wan, X. Gong, A. Riddle, A. Craig, J. Struve, L.S. Sherman, et al. 2008. Arrested oligodendrocyte lineage maturation in chronic perinatal white matter injury. *Ann. Neurol.* 63:520–530. https://doi.org/10.1002/ana.21359

Shi, Y., Q. Shao, Z. Li, G.A. Gonzalez, F. Lu, D. Wang, Y. Pu, A. Huang, C. Zhao, C. He, et al. 2018. Myt1L Promotes Differentiation of Oligodendrocyte Precursor Cells and is Necessary for Remyelination After Lysolecithin-Induced Demyelination. *Neurosci. Bull.* 34:247–260. https://doi.org/10.1007/s12264-018-0207-9

Simons, F.E. 2002. H1-antihistamines in children. *Clin. Allergy Immunol.* 17:437–464.

Simons, F.E., and K.J. Simons. 2008. H1 antihistamines: current status and future directions. *World Allergy Organ. J.* 1:145–155. https://doi.org/10.1097/WOX.0b013e318186fb3a

Skoff, R.P., D.A. Bessert, J.D. Barks, D. Song, M. Cerghet, and F.S. Silverstein. 2001. Hypoxic-ischemic injury results in acute disruption of myelin gene expression and death of oligodendroglial precursors in neonatal mice. *Int. J. Dev. Neurosci.* 19:197–208. https://doi.org/10.1016/S0736-5748(00)00075-7

Slaughter, J.L., M.R. Stenger, P.B. Reagan, and S.R. Jadcherla. 2016. Neonatal Histamine-2 Receptor Antagonist and Proton Pump Inhibitor Treatment at United States Children's Hospitals. *J. Pediatr.* 174:63–70.e3. https://doi.org/10.1016/j.jpeds.2016.03.059

Traiffort, E., H. Pollard, J. Moreau, M. Ruat, J.C. Schwartz, M.I. Martinez-Mir, and J.M. Palacios. 1992. Pharmacological characterization and autoradiographic localization of histamine H2 receptors in human brain identified with [125I]iodoaminopotentidine. *J. Neurochem.* 59:290–299. https://doi.org/10.1111/j.1471-4159.1992.tb08903.x

Wang, F., Y.J. Yang, N. Yang, X.J. Chen, N.X. Huang, J. Zhang, Y. Wu, Z. Liu, X. Gao, T. Li, et al. 2018. Enhancing Oligodendrocyte Myelination Rescues Synaptic Loss and Improves Functional Recovery after Chronic Hypoxia. *Neuron.* 99:689–701.e5. https://doi.org/10.1016/j.neuron.2018.07.017

Xu, X., Y. Song, Y. Li, J. Chang, H. Zhang, and L. An. 2010. The tandem affinity purification method: an efficient system for protein complex purification and protein interaction identification. *Protein Expr. Purif.* 72:149–156. https://doi.org/10.1016/j.pep.2010.04.009

Yang, Z., M. Watanabe, and A. Nishiyama. 2005. Optimization of oligodendrocyte progenitor cell culture method for enhanced survival. *J. Neurosci. Methods.* 149:50–56. https://doi.org/10.1016/j.jneumeth.2005.05.003

Ye, F., Y. Chen, T. Hoang, R.L. Montgomery, X.H. Zhao, H. Bu, T. Hu, M.M. Taketo, J.H. van Es, H. Clevers, et al. 2009. HDAC1 and HDAC2 regulate oligodendrocyte differentiation by disrupting the beta-catenin-TCF interaction. *Nat. Neurosci.* 12:829–838. https://doi.org/10.1038/nn.2333

Yıldız, E.P., B. Ekici, and B. Tatlı. 2017. Neonatal hypoxic ischemic encephalopathy: an update on disease pathogenesis and treatment. *Expert Rev. Neurother.* 17:449–459. https://doi.org/10.1080/14737175.2017.1259567

Yuan, Y., Y. Zheng, X. Zhang, Y. Chen, X. Wu, J. Wu, Z. Shen, L. Jiang, L. Wang, W. Yang, et al. 2017. BNIP3L/NIX-mediated mitophagy protects against ischemic brain injury independent of PARK2. *Autophagy.* 13:1754–1766. https://doi.org/10.1080/15548627.2017.1357792

Zhao, Y.Y., Y. Yuan, Y. Chen, L. Jiang, R.J. Liao, L. Wang, X.N. Zhang, H. Ohtsu, W.W. Hu, and Z. Chen. 2015. Histamine promotes locomotion recovery after spinal cord hemisection via inhibiting astrocytic scar formation. *CNS Neurosci. Ther.* 21:454–462. https://doi.org/10.1111/cns.12379

Zhou, L., C.Y. Shao, S.M. Xu, J. Ma, Y.J. Xie, L. Zhou, P. Teng, Y. Wang, M. Qiu, and Y. Shen. 2014. GSK3β promotes the differentiation of oligodendrocyte precursor cells via β-catenin-mediated transcriptional regulation. *Mol. Neurobiol.* 50:507–519. https://doi.org/10.1007/s12035-014-8678-9

Zhou, Y., J. Zhang, L. Wang, Y. Chen, Y. Wan, Y. He, L. Jiang, J. Ma, R. Liao, X. Zhang, et al. 2017. Interleukin-1β impedes oligodendrocyte progenitor cell recruitment and white matter repair following chronic cerebral hypoperfusion. *Brain Behav. Immun.* 60:93–105. https://doi.org/10.1016/j.bbi.2016.09.024

Supplemental material

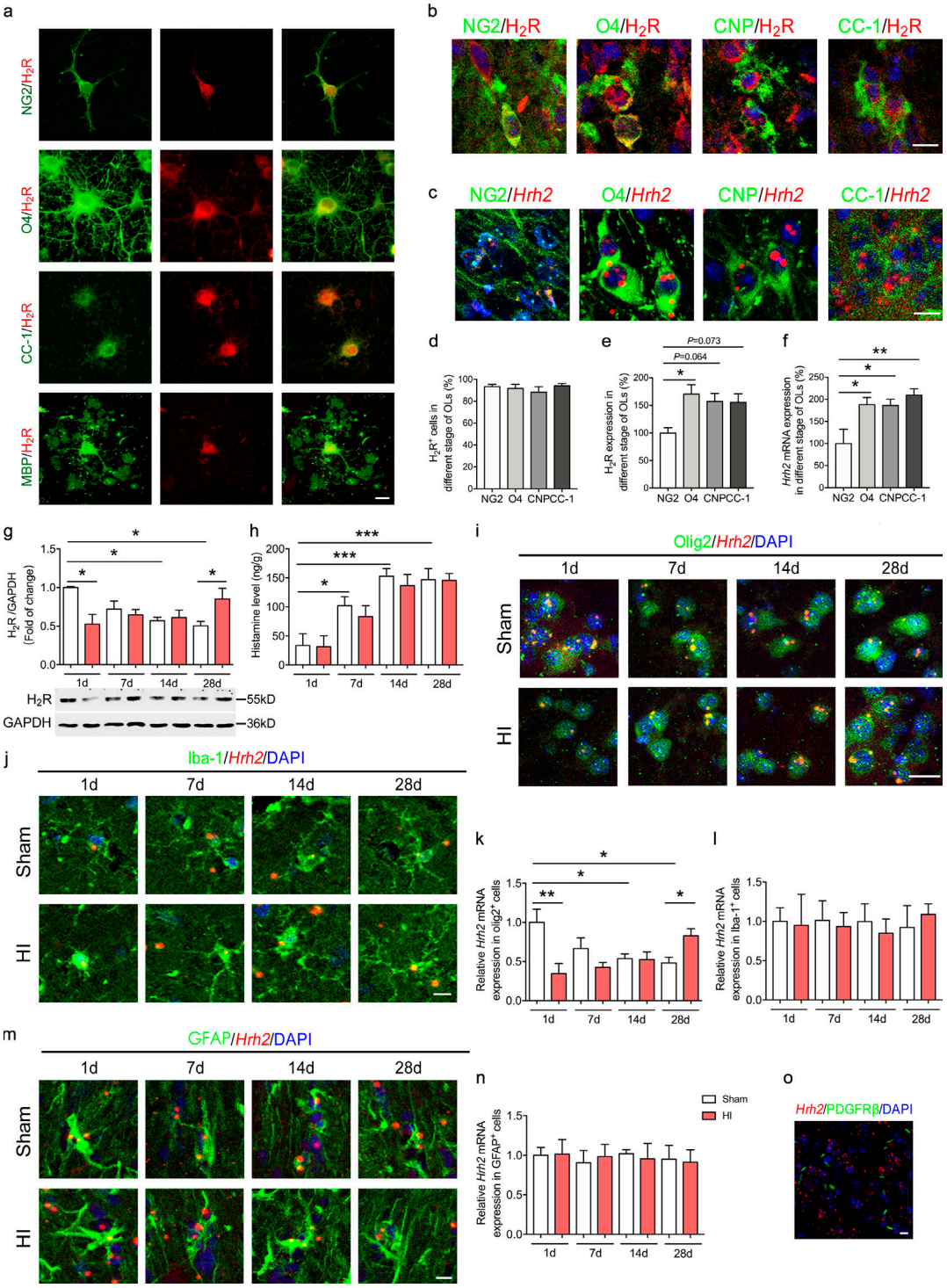

Figure S1. **H_2R expression in the OL lineages and in different types of cells in the white matter following neonatal HI. (a)** The primary cultured OPCs were differentiated with incubation in T3 (40 ng/ml) and CNTF (10 ng/ml) for 3 d (differentiating OLs) or 6 d (mature OLs). Immunocytochemical visualization of H_2R expression in $NG2^+$ OPCs, $O4^+$ differentiating OLs, $CC\text{-}1^+$, or MBP^+ mature OLs. **(b, d, and e)** Immunohistochemical visualization of H_2R protein as well as the quantification of the percentage of H_2R^+ cells and the intensity of H_2R protein expression in NG2, O4, CNP, and $CC\text{-}1^+$ OLs in the corpus callosum of the mouse brain. Green: NG2 labels OPCs; O4 and CNP label differentiating OLs; CC-1 labels mature OLs. Red, H_2R; blue, DAPI. *n* = 4 or 5 from three independent experiments. **(c and f)** In situ hybridization of *Hrh2* mRNA by RNAscope and the quantification of the *Hrh2* mRNA expression intensity in NG2, O4, CNP, and $CC\text{-}1^+$ OLs in the corpus callosum of the mouse brain. Green: NG2 labels OPCs; O4 and CNP label differentiating OLs, CC-1 labels mature OLs. Red, *Hrh2* mRNA; blue, DAPI. *n* = 4 or 5 from three independent experiments. **(g)** Western blot analysis showing the protein expression of H_2R in the corpus callosum at 1 d, 7 d, 14 d, and 28 d after neonatal HI. **(h)** ELISA of histamine level in the corpus callosum at 1 d, 7 d, 14 d, and 28 d after neonatal HI. **(i–n)** In situ hybridization of *Hrh2* mRNA by RNAscope and the quantification of the *Hrh2* mRNA expression intensity in OLs ($Olig2^+$, i and k), microglia ($Iba\text{-}1^+$, j and l), and astrocyte ($GFAP^+$, m and n) in the corpus callosum after HI. **(o)** In situ hybridization of *Hrh2* mRNA in pericytes by RNAscope together with immunostaining of PDGFRβ. *n* = 4 or 5 mice for each group from two independent experiments. All scale bars, 20 µm. *, $P < 0.05$; **, $P < 0.01$; ***, $P < 0.001$.

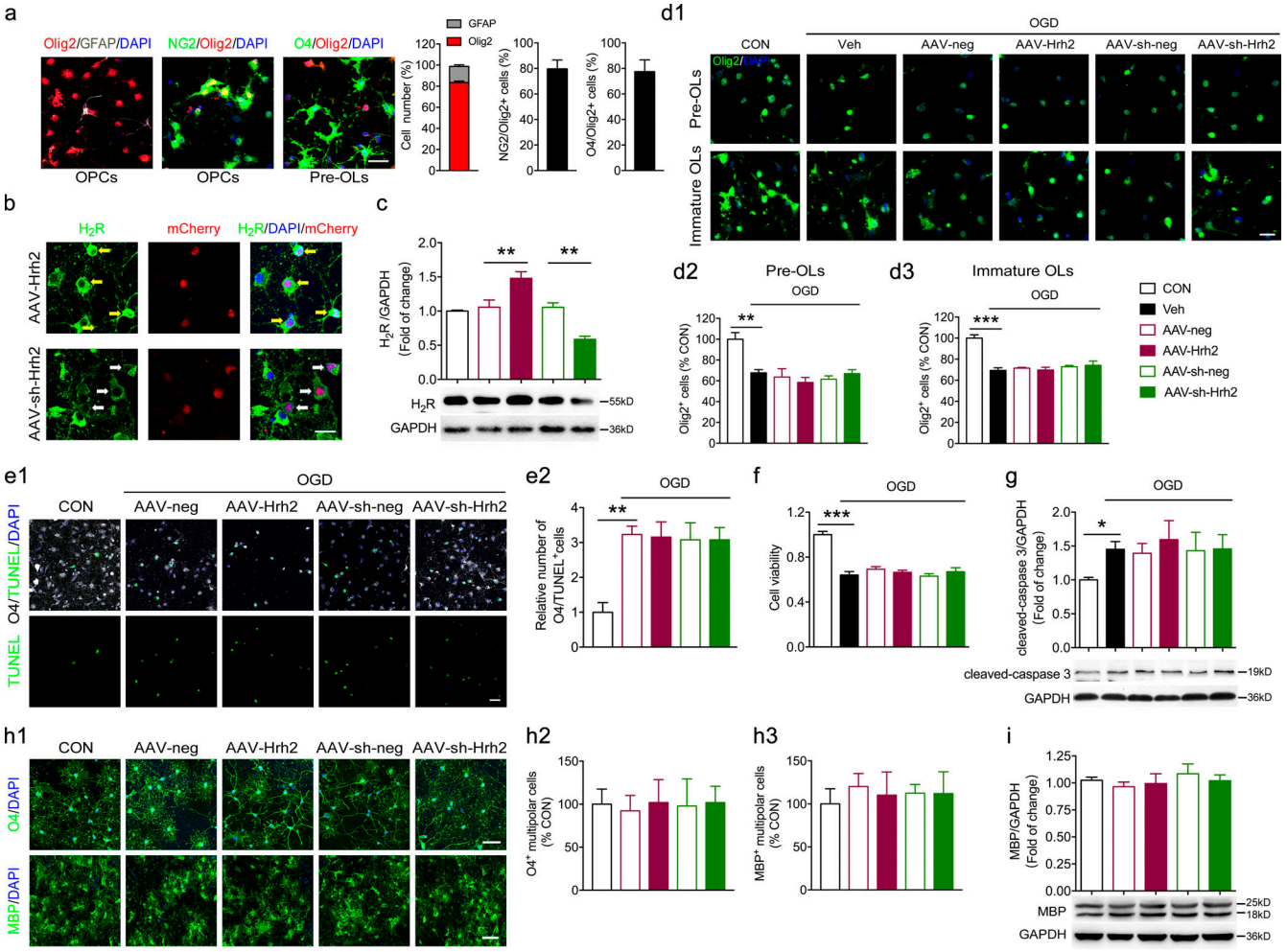

Figure S2. **The effect of overexpression and knockdown of H_2R on cultured OLs. (a)** The primary cultured OPCs were differentiated into preOLs with incubation in T3 (40 ng/ml) and CNTF (10 ng/ml) for 2 d. Immunocytochemical staining of Olig2 together with GFAP, NG2, or O4 was performed to confirm the purity of OPCs (NG2) or preOLs (O4), respectively. The percentage of $Olig2^+$ OL lineage (and the percentage of astrocytes) in cultured cells as well as the percentage of $NG2^+$ OPC and $O4^+$ multipolar preOLs among all the $Olig2^+$ OLs were quantified. Scale bar, 50 µm. **(b and c)** The AAV-Hrh2 and AAV-sh-Hrh2 infection efficiency was evaluated by immunocytochemical staining in primary cultured OLs (b) and Western blot analysis of oli-neu cells (c). **(d1–d3)** The primary cultured OPCs were differentiated into preOLs or immature OLs with incubation in T3 (40 ng/ml) and CNTF (10 ng/ml) for 2 d or 4 d, respectively. These preOLs or immature OLs transfected with AAV-Hrh2 or AAV-sh-Hrh2 were subjected to OGD/reperfusion. The total number of $Olig2^+$ OL lineages was quantified at 24 h after reperfusion. Scale bar, 20 µm. **(e1, e2, f, and g)** The primary cultured OPCs or oli-neu cells were differentiated into preOLs with incubation in T3 (40 ng/ml) and CNTF (10 ng/ml) for 2 d. These preOLs infected with AAV-Hrh2 or AAV-sh-Hrh2 were subjected to OGD/reperfusion. **(e1 and e2)** Immunocytochemical visualization and the quantification of numbers of O4 and TUNEL double-positive OLs at 24 h after reperfusion. **(f)** Cell viability tested by MTT assay in oli-neu cells at 24 h after reperfusion. **(g)** Western blot analysis of cleaved-caspase3 in oli-neu cells at 24 h after reperfusion. **(h1–h3 and i)** The primary cultured OPCs or oli-neu cells were differentiated into preOLs or immature OLs with incubation in T3 (40 ng/ml) and CNTF (10 ng/ml) for 2 d or 4 d, respectively. These preOLs or immature OLs transfected with AAV-Hrh2 or AAV-sh-Hrh2 were allowed further differentiation for 1 d. Immunocytochemical visualization (h1) and the quantification of numbers of $O4^+$ multipolar cells differentiated from preOLs (h2). Immunocytochemical visualization (h1) and the quantification of numbers of MBP^+ multipolar cells differentiated from immature OLs (h3). Scale bar, 50 µm. **(i)** Western blot analysis of the MBP expression in oli-neu cells differentiated from immature stage. *n* = 4–6 trials from at least three independent experiments. *, $P < 0.05$; **, $P < 0.01$; ***, $P < 0.001$. CON, control; Veh, vehicle.

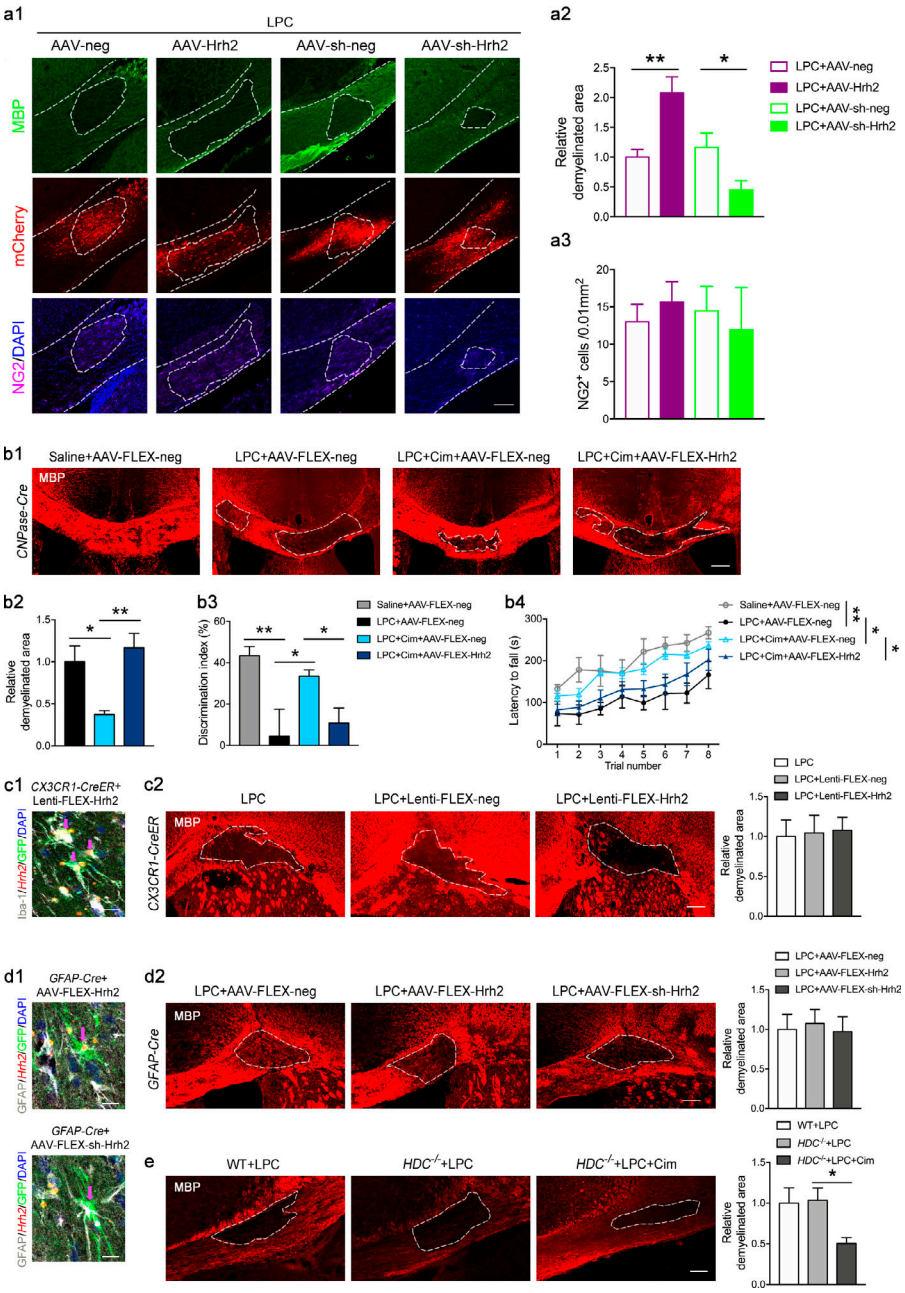

Figure S3. **The effect of overexpression and knockdown of H_2R on remyelination and neurological function in LPC-induced demyelination model. (a1–a3)** Mice were injected with AAV-Hrh2 or AAV-sh-Hrh2 to overexpress or knock down H_2R, and then received the LPC injection in the right side of the corpus callosum. Immunocytochemical visualization (a1) and quantification of demyelinated area in MBP staining (a2) and $NG2^+$ OPCs (a3) in the LPC-induced demyelinated area at 10 dpl. The location of virus injection was indicated by mCherry (red) expression. **(b1–b4)** *CNPase-Cre* mice were injected with AAV-FLEX-Hrh2 to overexpress H_2R in differentiating OLs (or AAV-FLEX-neg as control), and then received LPC injection in two sites of the corpus callosum and cimetidine treatment (Cim). Immunocytochemical visualization (b1) and quantification of demyelinated area in MBP staining (b2) at 10 dpl, as well as motor coordination in rotarod test (b3) and cognitive ability in object recognition test (b4) at 9–10 dpl. **(c1 and c2)** *CX3CR1-Cre* mice were received Lenti-FLEX-Hrh2 infection to overexpress H_2R in microglia, and then received the LPC injection in the right side of corpus callosum. **(c1)** In situ hybridization of *Hrh2* mRNA by RNAscope, immunostaining of Iba-1 and GFP, and visualization of nuclei by DAPI in the corpus callosum to confirm the overexpression H_2R in microglia (arrows indicate the virus-infected $Iba\text{-}1^+$ microglia). **(c2)** Immunocytochemical visualization and quantification of demyelinated area in MBP staining at 10 dpl. **(d1 and d2)** *GFAP-Cre* mice received AAV-FLEX-Hrh2 or AAV-FLEX-sh-Hrh2 infection to overexpress or knock down H_2R, and then received the LPC injection in the right side of the corpus callosum. **(d1)** In situ hybridization of *Hrh2* mRNA by RNAscope, immunostaining of GFAP and GFP, and visualization of nuclei by DAPI in the corpus callosum to confirm the overexpression or knockdown of H_2R in astrocytes (arrows indicate the virus infected $GFAP^+$ astrocytes). **(d2)** Immunocytochemical visualization and quantification of demyelinated area in MBP expression at 10 dpl. **(e)** $HDC^{-/-}$ mice received the LPC injection in the right side of the corpus callosum and were administered cimetidine. Immunocytochemical visualization and quantification of demyelinated area in MBP staining at 10 dpl. All scale bars, 100 µm. *n* = 5 or 6 mice for each group from at least three independent experiments in a1–a3, b1, b2, c1, c2, d1, d2, and e; *n* = 7 or 8 mice for each group from at least three independent experiments in b3 and b4. The areas outlined by a dashed line indicate the demyelinated areas. *, $P < 0.05$; **, $P < 0.01$.

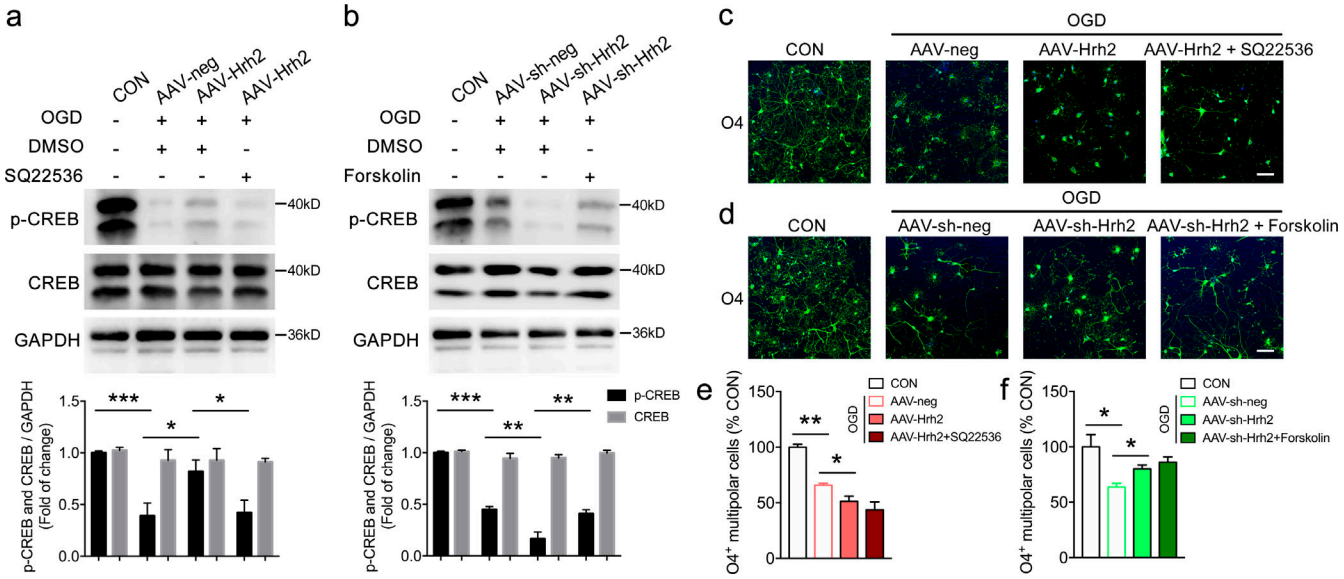

Figure S4. **The effect of overexpression and knockdown of H_2R on the AC/cAMP/CREB pathway during OL differentiation after OGD insult.** **(a)** Western blot analysis of phosphorylation of CREB (p-CREB) and CREB following AAV-Hrh2 infection and SQ22536 treatment in oli-neu cells exposed to OGD/reperfusion. **(b)** Western blot analysis of p-CREB and CREB following AAV-sh-Hrh2 infection and forskolin treatment in oli-neu cells exposed to OGD/reperfusion. **(c and e)** Immunocytochemical visualization and quantification of $O4^+$ multipolar differentiating OLs following AAV-Hrh2 infection and SQ22536 treatment. **(d and f)** Immunocytochemical visualization and quantification of $O4^+$ multipolar differentiating OLs following AAV-sh-Hrh2 infection and forskolin treatment. *n* = 3 or 4 from three independent experiments. Scale bar, 50 µm. *, P < 0.05; **, P < 0.01; ***, P < 0.001. CON, control.

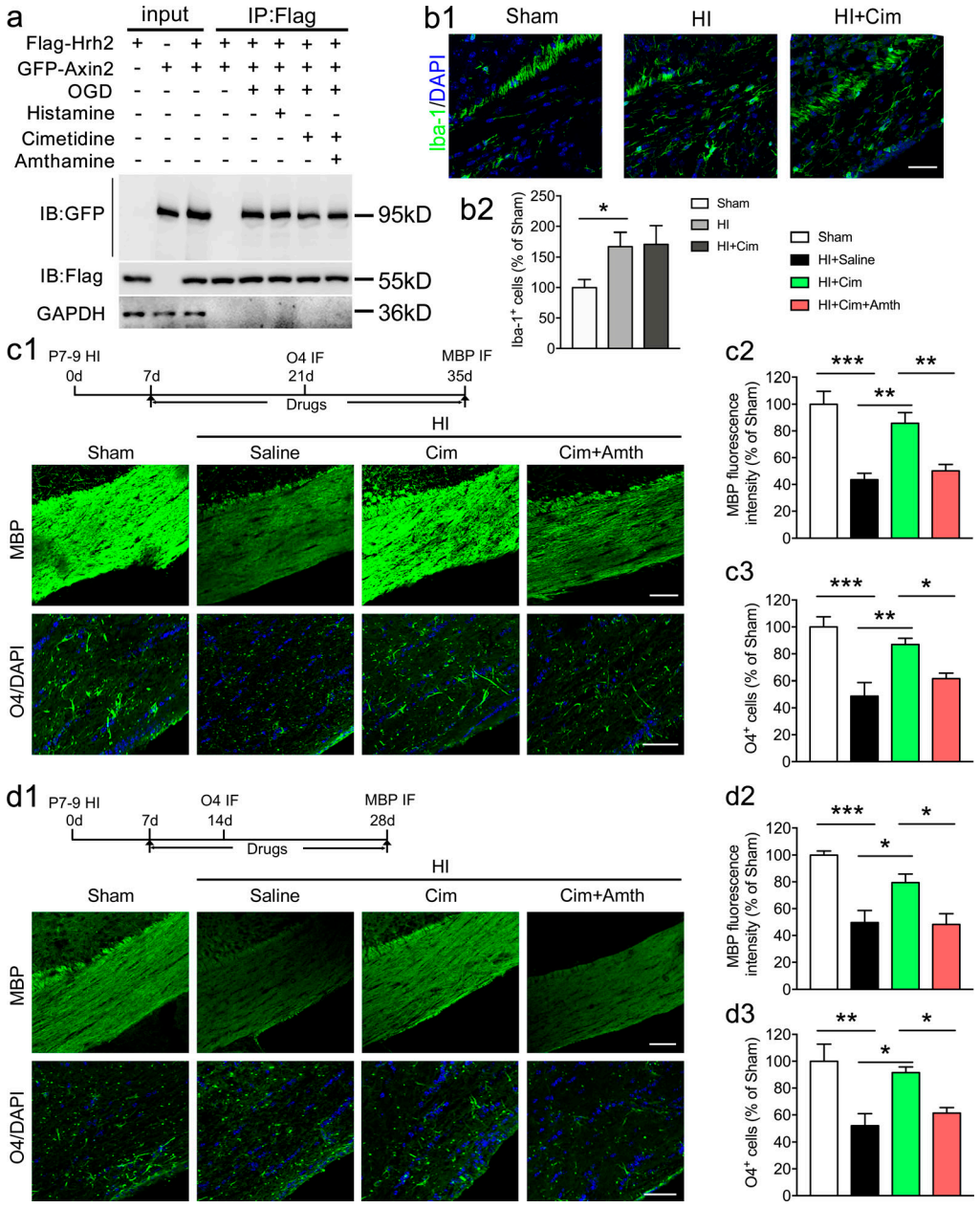

Figure S5. **Effects of H_2R antagonist on the interaction between H_2R and Axin2 or on the WMI in neonatal HI mice. (a)** Representative coimmunoprecipitation results showing the effect of histamine, H_2R antagonist cimetidine (Cim), or H_2R agonist amthamine (Amth) on the interaction of H_2R with Axin2 following OGD/reperfusion. **(b1 and b2)** Neonatal mice were subjected to unilateral common carotid artery ligation plus inhalational hypoxia and received cimetidine administration. Immunohistochemical visualization (b1) and quantification of Iba-1 expression (b2) indicating microglia activation at 14 d after HI. *n* = 4 mice for each group from two independent experiments. **(c1–c3)** The H_2R antagonist cimetidine alone or together with H_2R agonist amthamine was administered by a delayed (7–35 d, a–d) approach after HI surgery. Immunohistochemical visualization (c1) and quantification of MBP expression at 35 d (c2) and $O4^+$ multipolar differentiating OLs at 21 d (c3). *n* = 7 mice for each group from three independent experiments. **(d1–d3)** The H_2R antagonist cimetidine alone or together with H_2R agonist amthamine was administered by a shortened and delayed (7–28 d) approach after HI surgery. Immunohistochemical visualization (d1) and quantification of MBP expression at 28 d (d2) and $O4^+$ multipolar differentiating OLs at 14 d (d3). *n* = 6 mice for each group from three independent experiments. Scale bar, 100 µm. *, P < 0.05; **, P < 0.01; ***, P < 0.001. IB, immunoblot; IF, immunofluorescence staining; IP, immunoprecipitation.